

# Accurate Machine Learned Quantum-Mechanical Force Fields for Biomolecular Simulations

Oliver T. Unke<sup>1,2,3\*</sup>    Martin Stöhr<sup>4</sup>    Stefan Ganschä<sup>1</sup>    Thomas Unterthiner<sup>1</sup>  
Hartmut Maennel<sup>1</sup>    Sergii Kashubin<sup>1</sup>    Daniel Ahlin<sup>1</sup>    Michael Gastegger<sup>2,3,5</sup>  
Leonardo Medrano Sandonas<sup>4</sup>    Alexandre Tkatchenko<sup>4\*</sup>    Klaus-Robert Müller<sup>1,2,6,7,8\*</sup>

<sup>1</sup>Google Research, Brain team

<sup>2</sup>Machine Learning Group, Technische Universität Berlin, 10587 Berlin, Germany

<sup>3</sup>DFG Cluster of Excellence “Unifying Systems in Catalysis” (UniSysCat), Technische Universität Berlin, 10623 Berlin, Germany

<sup>4</sup>Department of Physics and Materials Science, University of Luxembourg, L-1511 Luxembourg City, Luxembourg

<sup>5</sup>BASLEARN – TU Berlin/BASF Joint Lab for Machine Learning, Technische Universität Berlin, 10587 Berlin, Germany

<sup>6</sup>Department of Artificial Intelligence, Korea University, Anam-dong, Seongbuk-gu, Seoul 02841, Korea

<sup>7</sup>Max Planck Institute for Informatics, Stuhlsatzenhausweg, 66123 Saarbrücken, Germany

<sup>8</sup>BIFOLD – Berlin Institute for the Foundations of Learning and Data, Berlin, Germany

\*To whom correspondence should be addressed

E-mail: oliver.unke@gmail.com, alexandre.tkatchenko@uni.lu, klaus-robert.mueller@tu-berlin.de

## Abstract

Molecular dynamics (MD) simulations allow atomistic insights into chemical and biological processes. Accurate MD simulations require computationally demanding quantum-mechanical calculations, being practically limited to short timescales and few atoms. For larger systems, efficient, but much less reliable empirical force fields are used. Recently, machine learned force fields (MLFFs) emerged as an alternative means to execute MD simulations, offering similar accuracy as *ab initio* methods at orders-of-magnitude speedup. Until now, MLFFs mainly capture short-range interactions in small molecules or periodic materials, due to the increased complexity of constructing models and obtaining reliable reference data for large molecules, where long-ranged many-body effects become important. This work proposes a general approach to constructing accurate MLFFs for large-scale molecular simulations (GEMS) by training on “bottom-up” and “top-down” molecular fragments of varying size, from which the relevant physicochemical interactions can be learned. GEMS is applied to study the dynamics of alanine-based peptides and the 46-residue protein crambin in aqueous solution, allowing nanosecond-scale MD simulations of >25k atoms at essentially *ab initio* quality. Our findings suggest that structural motifs in peptides and proteins are more flexible than previously thought, indicating that simulations at *ab initio* accuracy might be necessary to understand dynamic biomolecular processes such as protein (mis) folding, drug–protein binding, or allosteric regulation.

## Introduction

Molecular dynamics (MD) simulations allow to determine the motion of individual atoms in chemical and biological processes, enabling mechanistic insights into molecular properties and functions, as well as providing a detailed interpretation of experimental studies. MD simulations require a reliable model of the forces acting on each atom at every time step of the dynamics [1]. It is most desirable to obtain atomic forces from accurate solutions to the many-body Schrödinger equation [2], but this is only feasible for short MD simulations of few atoms for the foreseeable future [3].

For larger systems, it is common practice to derive the forces from empirical models of the potential energy. Such force fields (FFs) approximate chemical interactions with computationally efficient terms and enable MD simulations of millions of atoms [4] for up to several milliseconds of dynamics [5]. A disadvantage of FFs is their limited accuracy due to the neglect of important quantum-mechanical effects, such as changes to hybridization states, interactions between orbitals delocalized over several atoms, or electronic correlations between distant molecular fragments. Further, many FFs require a predetermined covalent bonding structure, preventing bond breaking and formation. When additional accuracy and flexibility is required, for example to study an enzymatic reaction, a possible alternative are quantum mechanics/molecular mechanics (QM/MM) simulations [3, 6]: The system is divided into a small QM region modelled with *ab initio* methods (e.g. substrate and active site of an enzyme) and an MM region (e.g. the remaining protein and solvent molecules) described with an FF. However, the high computational cost associated with an accurate treatment of the QM region and the fact that it is often unclear which atoms need to be included for an adequate description of the process of interest [7] may limit the applicability of QM/MM methods.

In recent years, machine learned force fields (MLFFs) have emerged as an alternative means to execute MD simulations, combining the computational efficiency of traditional FFs with the high accuracy of quantum-chemistry methods [8]. To construct an MLFF, a machine learning (ML) model is trained on *ab initio* reference data to predict energies and forces from atomic positions – without the need to explicitly solve the Schrödinger equation outside of the reference data. MLFFs have led to numerous

insights, e.g. regarding reaction mechanisms [9], or the importance of quantum-mechanical effects for the dynamics of molecules [10]. Despite these successes, until now, MLFFs have been applied primarily to MD simulations of small to medium-sized systems (tens of atoms), or periodic materials (e.g. metallic copper) [11]. Applications to large heterogeneous systems, like proteins or other biologically relevant systems, have remained elusive, due to the increased complexity of constructing physically-informed ML architectures and obtaining reliable reference data for long-range interactions, which are known to play a key role in biomolecular dynamics [12, 13].

This work proposes a general approach to constructing accurate machine-learned force fields for large-scale molecular simulations (GEMS). Based on the divide-and-conquer principle, MLFFs for large heterogeneous systems are trained on molecular fragments of varying size, which cover the relevant chemical interactions, but are still amenable to electronic-structure calculations. From this fragment data, the model infers to recombine the original system, which allows GEMS to successfully address the long-standing challenge of biomolecular simulations at *ab initio* quality (Fig. 1A). While MLFFs can successfully learn local chemical interactions from small molecules [14], a sufficient number of larger fragments is needed to learn long-range effects necessary to generalize to larger systems and achieve high prediction accuracy (0.450 meV/atom for energies and 36.704 meV/Å for forces). In this work, we rely on the recently proposed SpookyNet architecture [15], which models dispersion and electrostatics explicitly by embedding physically motivated interaction terms into the ML architecture and learning their parameters from reference data. In addition, an empirical term for short-ranged repulsion between atomic nuclei increases the robustness of the model for strong bond distortions. SpookyNet also includes a mechanism to describe effects like non-local charge transfer, which other MLFFs (with some exceptions [16]) are typically unable to. Taken together, these components enable the model to generalize to larger molecules when trained on appropriate reference data. However, ultimately, the quality and reliability of an MLFF should be judged by its predictions of experimental measurements – for example, we show that GEMS is able to quantitatively reproduce experimental results regarding the helix stability of polyalanine systems at different temperatures and correctly describe infrared

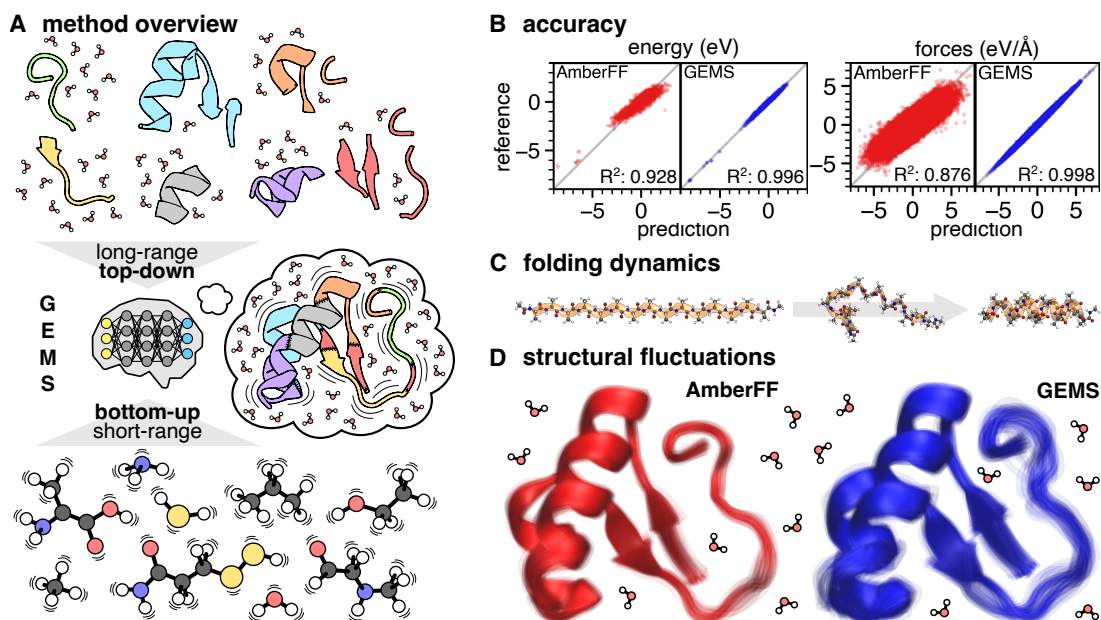


Figure 1: **Insights from GEMS simulations.** (A) Overview of the GEMS method. Different interaction scales on the potential-energy surface (PES) of a large system are learned from a combination of *ab initio* reference data for top-down and bottom-up fragments. The resulting model is able to accurately reconstruct the PES of the molecular system and then used to study its dynamics. (B) Prediction accuracy for energies and forces of AceAla<sub>15</sub>Nme conformations of GEMS compared to AmberFF [17] with respect to the PBE0/def2-TZVPP+MBD [18–21] reference. (C) GEMS simulations show that the folding of AceAla<sub>15</sub>Nme from a fully extended structure (left) to a helical conformation (right) occurs via intermediate conformations characterized by hydrogen bonding between backbone atoms of adjacent residues (middle). (D) Overlay of representative conformations (obtained from cluster analysis) sampled during an aggregated 10 ns of dynamics of crambin in aqueous solution. Simulations with GEMS (blue) lead to greater structural fluctuations compared to AmberFF (red), indicating that the protein is more flexible.

peak positions of water for a solvated protein.

GEMS is applied to MD simulations of model peptides and the 46-residue protein *crambin* in aqueous solution (>25k atoms). When comparing to conventional force fields, such as AMBER99SB-ILDN [17] (AmberFF), GEMS approximates energies and forces computed from density-functional theory much more closely (Fig. 1B). Interestingly, our findings reveal previously unknown intermediates in the folding pathway of poly-alanine peptides (Fig. 1C) and a dynamical equilibrium between  $\alpha$ - and  $3_{10}$ -helices. In the simulations of solvated crambin, GEMS indicates that protein motions are qualitatively different and more flexible when compared to computations with a conventional FF (Fig. 1D), showing contrasting short

and long timescale dynamics. These results suggest that simulations at *ab initio* accuracy may be necessary to fully understand dynamic processes like protein (mis)folding, drug–protein binding, or allosteric regulation.

## Results

### Machine learning force fields for large systems

We start by generating reference data for smaller molecular fragments in order to train an MLFF, where the learned model accurately reflects the full large system. There are

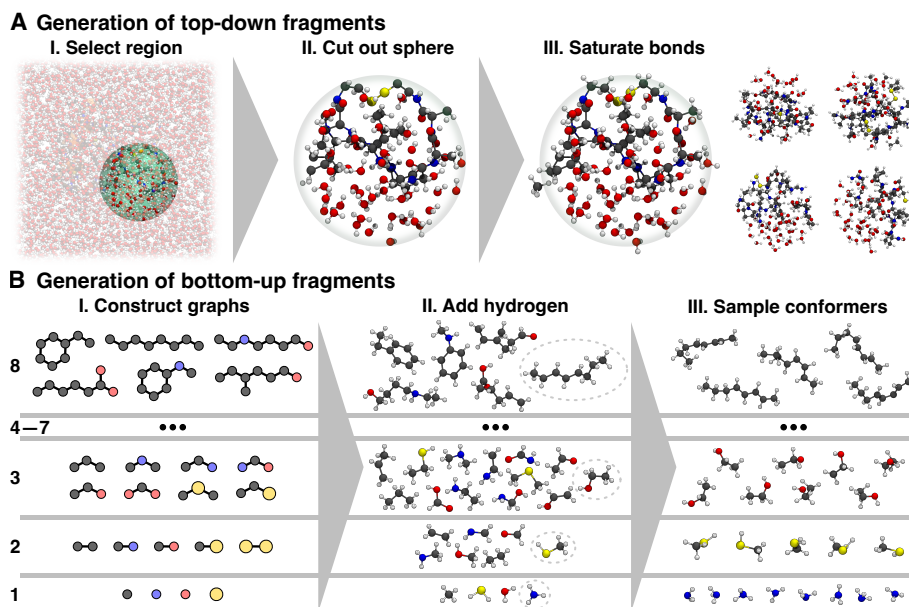


Figure 2: **Generation of top-down and bottom-up fragments.** (A) Top-down fragments are generated by cutting out a spherical region around an atom (including solvent molecules) and saturating all dangling bonds (the right side shows four top-down fragments generated from different regions). They are crucial for learning weak but long-ranged interactions, which are important for the dynamics of large systems. (B) Bottom-up fragments are generated by constructing chemical graphs consisting of one to eight non-hydrogen atoms (not all possible graphs are shown). The graphs are then converted to three-dimensional structures by adding hydrogen atoms. Due to their small size, multiple *ab initio* calculations for many different conformers of each generated structure can be performed, allowing extensive sampling of the potential energy surface which is necessary for training robust models.

several strategies to achieve this goal. On one hand, the model needs to be able to learn all relevant chemical interactions that are necessary to reconstruct a complete and accurate picture of the system of interest from the fragment data. This is important to capture weak, but long-ranged interactions, which collectively dominate e.g. relative energy differences of different conformations of large molecules. On the other hand, it is necessary to prevent “holes” in the potential energy surface (PES) [22] – regions with low potential energy corresponding to unphysical structures, e.g. featuring unnaturally large or short bond lengths. The existence of holes in the PES prevents stable MD simulations, because long trajectories eventually may become trapped by such artefacts and behave unphysically [23]. To achieve both requirements, we propose the use of two complementary methods to construct fragments, which

allow models to learn different aspects of the PES of large systems. The first method follows a top-down approach, where fragments are constructed by “cutting out” spherical regions of the system of interest, which also includes solvent molecules in the condensed phase (Fig. 2A) [24]. They are chosen as large as possible to sample important long-range effects, but still small enough such that reference energies and forces computed with quantum chemistry methods are accessible in a reasonable time. As our tests on poly-alanine systems demonstrate (see below), the top-down fragments we choose are sufficiently large for the systems studied in this work.

Since it is difficult to collect enough reference data for the large top-down fragments to train robust models, they are enriched by smaller fragments, for which data points for many different conformations can be collected. Start-

ing from single atoms, molecules similar to local bonding patterns of the system of interest [14] are systematically constructed by growing chemical graphs in a bottom-up fashion (Fig. 2B). By limiting the size of these fragments, it is possible to sample many different conformations, allowing models to learn the effects of strong distortions in local structural patterns, which is key to preventing holes in the PES. As a result, the combination of bottom-up and top-down fragments enables learning accurate and robust MLFFs for large systems.

## Poly-alanine systems

We apply GEMS to predict the properties and dynamics of several peptides consisting primarily of alanine. These are popular model systems for proteins and well studied both theoretically and experimentally. In addition, by limiting the number of residues, it is still possible to perform electronic-structure calculations for the full system. Thus, the predictions of an ML model trained only on fragment data can be directly compared to reference calculations, which allows to verify the ability of GEMS to reconstruct the properties of larger systems from the chemical knowledge extracted from smaller molecules.

As a first test case, we consider the cooperativity between hydrogen bonds in poly-alanine peptides capped with an N-terminal acetyl group and a protonated lysine residue at the C-terminus ( $\text{AceAla}_n\text{Lys} + \text{H}^+$ ). In  $\alpha$ -helices, the local dipole moments of hydrogen bonds formed between backbone peptide groups are aligned, leading to a cooperative polarization effect [26]. Thus, the relative stabilization energy of an  $\alpha$ -helix compared to a fully extended structure (FES) fluctuates non-trivially with helix length and is a challenging prediction task. We find that GEMS closely agrees with the reference *ab initio* method, demonstrating that large-scale effects can be learned effectively from fragment data (Fig. 3A).

Alanine-based peptides have a strong tendency to form helical structures. While short isolated helices are only marginally stable in solution,  $\text{AceAla}_{15}\text{Lys} + \text{H}^+$  is known to form stable helices in gas phase. Experimental results suggest that  $\text{AceAla}_{15}\text{Lys} + \text{H}^+$  remains helical up to temperatures of  $\sim 725$  K [27], allowing a direct comparison with theoretical predictions. By running GEMS simulations at different temperatures, we confirm that the peptide remains primarily helical up to 700 K, but forms

a random coil at 800 K (see supplementary video 1 at <https://youtu.be/QZ1c3a40jJk>). An analysis of the formed hydrogen bonds reveals that the average number of  $\alpha$ -helical hydrogen bonds decreases with increasing temperature (see Fig. S7A), while the number of  $3_{10}$ -helical hydrogen bonds remains almost constant until a sudden drop at 800 K (see Fig. 3B), which agrees with results from *ab initio* simulations [28]. Interestingly, the long-ranged interactions learned from top-down fragments seem to be crucial to reproduce the experimental results, as a model that was only trained on bottom-up fragments predicts reduced thermal stability (see Fig. S7B).

To investigate whether there are fundamental differences between GEMS and dynamics simulations performed with conventional FFs, we study the room temperature (300 K) folding process of a pure poly-alanine peptide capped with an N-terminal acetyl group and a C-terminal N-methyl amide group ( $\text{AceAla}_{15}\text{Nme}$ ) in gas phase. Starting from the FES, MD simulations with GEMS suggest that  $\text{AceAla}_{15}\text{Nme}$  has a strong tendency to form H-bonds between peptide groups of directly adjacent residues within the first  $\sim 100$  ps of dynamics. The formed arrangements exhibit a “wavy” structure and  $\phi$  and  $\psi$  backbone dihedral angles of  $\sim 0^\circ$  and  $\sim 0^\circ$ , which lie in a sparsely populated region of the Ramachandran plot. These intermediates are typically short-lived with lifetimes of  $\sim 25$ – $50$  ps, and fold readily into helical configurations via a characteristic twisting motion. There is still some controversy between theoretical and experimental results regarding the predominance of different helical conformations [29]. We find that there may be cases where no single motif is preferred: Once a helix is formed, its structure fluctuates between pure  $\alpha$ - and  $3_{10}$ -helices, as well as hybrids of both helix types (see supplementary video 2 at <https://youtu.be/ZuKW292DKKw> for a complete folding trajectory). A 10 ns trajectory of the helical state suggests a dynamical equilibrium with a  $\sim 38\%/62\%$  mixture of  $\alpha$ - and  $3_{10}$ -helices. In contrast, MD simulations with a conventional FF yield qualitatively different results, suggesting that a more rigid and primarily  $\alpha$ -helical configuration is formed from the FES without distinct structural intermediates (see Fig. 3C).

As a final test for the accuracy of GEMS, we compare the predictions of the ML model to *ab initio* data computed at the PBE0/def2-TZVPP+MBD [18–21] level of theory. To this end, we use 1554 and 1000  $\text{AceAla}_{15}\text{Nme}$

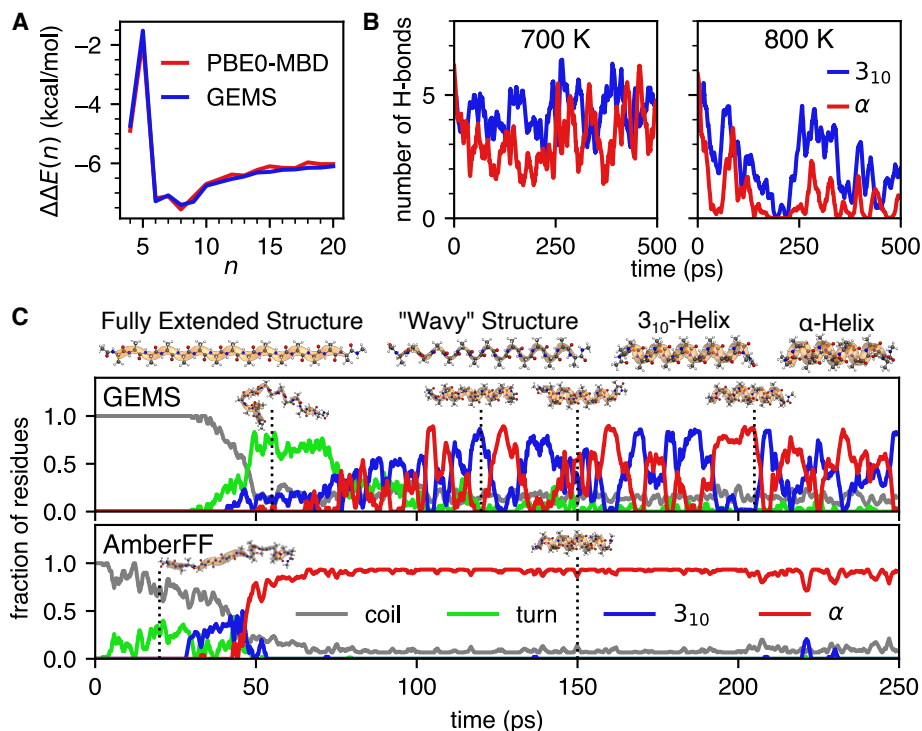


Figure 3: **Accurate simulations of poly-alanine systems with GEMS.** (A) Relative stabilization of the  $\alpha$ -helical conformation of AceAla $_n$ Lys + H $^+$  per added alanine residue. Shown here is the double difference  $\Delta\Delta E(n) = \Delta E(n) - \Delta E(n-1)$ , where  $\Delta E(n) = E_\alpha(n) - E_{\text{FES}}(n)$  is the relative energy of the  $\alpha$ -helical conformation and the fully extended structure (FES) of AceAla $_n$ Lys + H $^+$  in gas phase. The prediction of GEMS (blue) is compared to *ab initio* reference data computed at the PBE0-MBD [18–21] level of theory. (B) Number of  $\alpha$ - and  $3_{10}$ -helical H-bonds during MD simulations of helical AceAla $_{15}$ Lys + H $^+$  in gas phase at 700 K and 800 K with GEMS. The sharp drop in the number of H-bonds in the dynamics at 800 K indicates the formation of a random coil (see Fig. S7A for an extended version of this figure with a greater range of temperatures). (C) Secondary structural motifs determined by STRIDE [25] along typical folding trajectories of AceAla $_{15}$ Nme. Dotted vertical lines indicate the temporal position of the shown snapshots. The trajectory computed with GEMS (top) folds via a distinct “wavy” intermediate (classified primarily as “turn”) and settles into a dynamic equilibrium between  $3_{10}$ - and  $\alpha$ -helices. In contrast, the trajectory computed with the AmberFF (bottom) folds more directly and then stays primarily  $\alpha$ -helical (see Fig. S6 for an analysis of additional trajectories).

structures sampled from densely and sparsely populated regions (rare events) of the configurational space visited in 100 aggregated 250 ps MD trajectories (25 ns total) in the NVT ensemble at 300 K simulated with GEMS (see Section S4 for details). We find that predicted energies and forces are in good agreement with the reference values in both cases. For energies and forces, correlation coef-

ficients are  $R^2 = 0.996$  and  $R^2 = 0.998$ , respectively, and mean absolute errors (MAEs) are 0.450 meV/atom and 36.704 meV/Å. Again, we find that the inclusion of top-down fragments during training is crucial for high accuracy, as prediction errors for a model trained only on bottom-up fragments are much larger (see Fig. S4). In comparison, even though predictions with the conventional

AmberFF [17] are remarkably accurate with correlation coefficients of  $R^2 = 0.928$  (for energy) and  $R^2 = 0.876$  (for forces), the MAEs are much larger at 2.274 meV/atom and 329.328 meV/Å (distributions of predicted and reference energy values were shifted to have a mean of zero prior to computing MAEs in both cases, such that constant energy offsets between different methods do not influence the results). As a general trend, we observe that predictions with GEMS reproduce the reference across the whole range of values without the presence of a single outlier, whereas the AmberFF systematically under- and over-predicts small and large energy values, respectively (see Fig. 1B). These findings show that GEMS gives accurate predictions even for rare configurations and the simulated MD trajectories are essentially *ab initio* quality (see Figs. S2 and S3 for a more detailed analysis of correlations within the different subsets of configurations).

## Crambin

GEMS enables accurate molecular simulations in the condensed phase. The 46-residue protein crambin in aqueous solution (25257 atoms) is chosen as a model system. Crambin contains 15 out of the 20 natural amino acids and forms common structural motifs such as  $\beta$ -sheets,  $\alpha$ -helices, turns/loops, and disulfide bridges. To assess qualitative differences between simulations with a conventional FF (here, the AmberFF is chosen) and GEMS, we consider the power spectrum [33] computed from 125 ps of dynamics at a temporal resolution of 2.5 fs (Fig. 4A). The power spectrum is related to the internal motions of the system and reveals the dominant frequencies of molecular vibrations, which are influenced by the atomic structure and characteristic for the presence of certain functional groups. In comparison to the results obtained from the dynamics with a conventional FF, peaks in the power spectrum computed with GEMS are shifted towards lower wavenumbers and lie close to the frequency ranges expected from measured infrared spectra. For example, the dominant peaks above  $1000\text{ cm}^{-1}$  correspond to bending and stretching vibrations of water molecules, which are experimentally expected at around  $\sim 1600\text{ cm}^{-1}$  and  $\sim 3500\text{ cm}^{-1}$ , respectively [30], which is consistent with the GEMS spectrum. In contrast, the corresponding peaks for the conventional FF are blue-shifted several hundreds of wavenumbers. Additionally, peaks in the GEMS spectrum are broader, indi-

cating that the frequencies of characteristic vibrations are influenced stronger by intermolecular interactions, hence broadening their frequency range. Long-ranged interactions may particularly influence slow proteins motions, i.e. the low-frequency parts of the power spectrum, where notable differences between GEMS and AmberFF can be observed.

Similar to the results for AceAla<sub>15</sub>Nme, we find that in comparison to simulations with the AmberFF, crambin is more flexible in GEMS simulations (Fig. 1D). Although a straightforward quantitative comparison is not possible, qualitatively, the increased flexibility agrees more closely to structures modelled from nuclear magnetic resonance (NMR) spectroscopy measurements (see Fig. S5). The increased flexibility is also indicated by a Ramachandran map of the backbone dihedral angles of crambin (Fig. 4B), which shows that a wider range of values is sampled in simulations with GEMS. This becomes even more apparent by projecting the trajectories into a low-dimensional space that allows a direct visualization of the path taken through conformational space (Fig. 4C). However, a time-resolved analysis of the trajectories reveals that structural fluctuations with GEMS are only larger on timescales in excess of  $\sim 200$  ps (Fig. 4D). On shorter time scales on the other hand, the trend is reversed. This suggests that there are qualitative differences between simulations with conventional FFs and GEMS on all timescales and simulations with *ab initio* accuracy might be crucial to fully understand protein dynamics.

## Discussion and conclusion

Modeling quantum-mechanical properties of large molecules is an outstanding challenge and it holds promise for broad application in chemistry, biology, pharmacology, and medicine. We have developed a general framework for constructing MLFFs – GEMS – for large molecular systems such as proteins by learning from *ab initio* reference data of small(er) fragments without the need to perform electronic-structure calculations for a whole protein – as the latter would constitute a computationally impractical task. The proposed divide-and-conquer strategy employing a library of  $\sim 3$  million DFT+MBD computations on fragments and using a machine learning model that incorporates physical constraints and long-range interactions

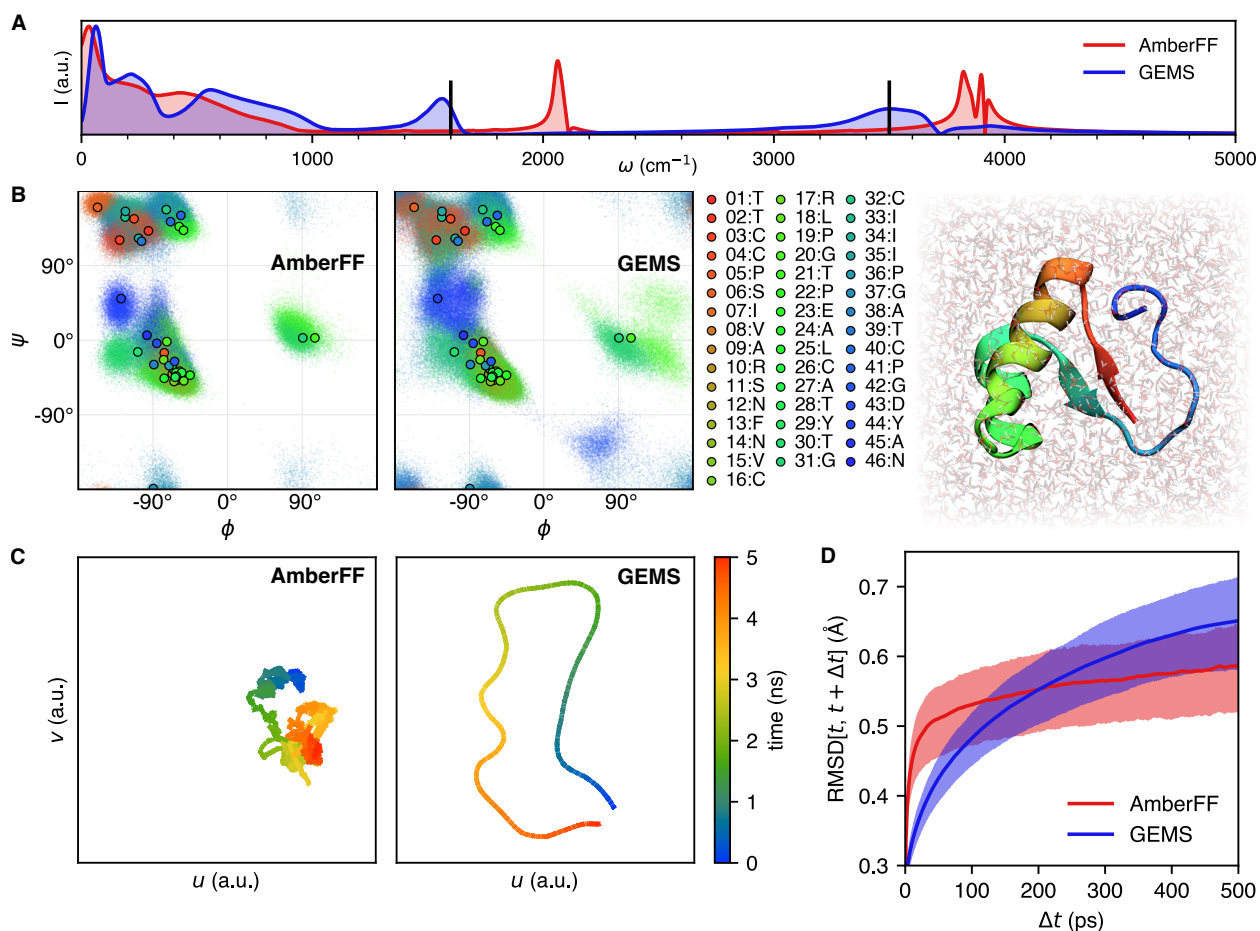


**Figure 4: Analysis of dynamics simulations of crambin in aqueous solution.** (A) Power spectrum of crambin in water obtained from 125 ps of dynamics computed with the AmberFF and GEMS. In the GEMS spectrum, peaks associated with bending and stretching vibrations of water molecules are closer to experimentally expected values at around  $\sim 1600 \text{ cm}^{-1}$  and  $\sim 3500 \text{ cm}^{-1}$  [30] (vertical black lines). (B) Ramachandran map for crambin (color-coded by residue number). The scatter shows the  $(\phi, \psi)$ -dihedral angles sampled during an aggregated 10 ns of dynamics, points with black outline show values of the crystal structure [31] for reference. Dynamics with GEMS (right) generally sample a broader distribution compared to AmberFF (left), indicating that the protein is more flexible. (C) Two-dimensional UMAP [32] projection of the path through conformational space sampled during a 5 ns trajectory of crambin in aqueous solution. Compared to the trajectory computed with the AmberFF, dynamics with GEMS sample a wider distribution and are less likely to revisit previously visited regions of conformational space. (D) Distribution of root mean square deviations (RMSDs, excluding hydrogen atoms) between conformations sampled at times  $t$  and  $t + \Delta t$ . Solid lines depict the mean, whereas the shaded region indicates the area between the 25th and 75th percentiles. Dynamics with the AmberFF (red) show larger structural fluctuations on short time scales, whereas fluctuations on longer timescales are larger for dynamics computed with GEMS (blue).



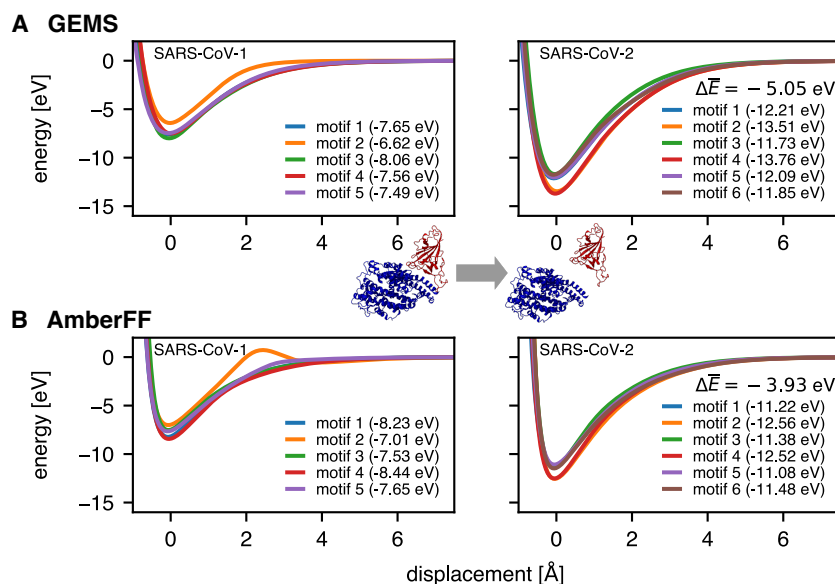


Figure 5: **Towards accurate quantum-mechanical protein–protein interactions: Gas-phase binding curves of the ACE2 (blue) and the receptor binding domain (RBD) of the SARS-CoV spike protein (red).** The ACE2 and RBD proteins are displaced along the line connecting their centers of mass relative to their equilibrium position in solution (computed with the AmberFF), keeping their internal structure fixed. Different binding motifs (taken from Ref. 34) are distinguished (values in brackets are the maximum well-depth for the corresponding motif). All energy values are referenced with respect to infinite separation of ACE2 and RBD. The displayed value  $\Delta\bar{E}$  gives the difference in well-depth (averaged over all binding motifs) between SARS-CoV-2 and SARS-CoV-1. The  $\Delta\Delta\bar{E}$  between AmberFF (B) and GEMS (A) is  $-1.11 \text{ eV}$ .

allows to efficiently construct MLFFs that accurately reflect the quantum-mechanical energies and atomic forces in large molecules. An interesting insight of our *ab initio* accurate simulations is that proteins are significantly more flexible than previously thought. These molecular fluctuations and associated low-frequency vibrations are expected to strongly contribute to dynamical processes such as protein folding, drug–protein binding, and allosteric regulation [35].

While our work focuses exclusively on the study of peptides and proteins, the proposed framework can be applied to any atomic system too large to study with *ab initio* methods. We find that even small poly-alanine peptides display qualitatively different dynamics when simulated with GEMS in comparison to dynamics with conventional FFs. For example, GEMS simulations

suggest that the folding of AceAla<sub>15</sub>Nme from the FES to a helical conformation occurs via short-lived intermediates characterized by hydrogen bonding between peptide groups of adjacent residues. Once a helix is formed, its structure fluctuates between  $3_{10}$ - and  $\alpha$ -helices in a dynamical equilibrium. This is in stark contrast to simulations with a conventional FF, where the peptide forms a rigid  $\alpha$ -helix without visiting a common intermediate. These results are reminiscent of the first MD study of a protein [36], which showed that proteins are less rigid than previously thought [37]. The current findings, already alluded to above, indicate that proteins might be even more flexible, and our simulations of crambin suggest that the general trend observed for peptides in gas phase also holds for proteins in solution. In particular, crambin samples a larger conformational

space in GEMS simulations and its backbone dihedral angles have broader distributions. Interestingly however, structural fluctuations on short time scales are reduced in comparison to simulations with a conventional FF. These observations show that there are qualitative differences in the dynamics of proteins when they are simulated with *ab initio* quantum-mechanical accuracy. We conjecture that these variations in the dynamics might be crucial for the understanding of effects like allostery, or processes like enzyme catalysis and protein (mis)folding. For example, a description of the potential energy at *ab initio* quality might be necessary to gain deeper insights into Levinthal’s paradox [38]. A promising avenue for future work is to extend GEMS to larger systems and longer timescales, for example by distributing GEMS simulations over multiple accelerators, which requires non-trivial modifications to the way the MLFF is evaluated. Other possible extensions to GEMS include incorporating nuclear quantum effects, which were demonstrated to significantly change the dynamics of small molecules [39]. It is likely that similar effects can be observed for larger systems.

Let us discuss some limits of MLFFs when compared to classical MD simulations. Although MLFFs are orders of magnitude more computationally efficient than *ab initio* calculations, their computational efficiency is lower than that of conventional FFs (as to be expected). For example, simulating a single timestep of NPT dynamics of crambin in aqueous solution on an NVIDIA A100 GPU with GEMS takes roughly  $\sim 500$  ms, whereas GROMACS [40] only requires  $\sim 2$  ms for a single time step with a conventional FF on similar hardware. Consequently, at this moment, GEMS simulations are limited to shorter time scales. In addition, evaluating MLFFs usually requires increased memory compared to conventional FFs, limiting the maximum system size that can be simulated with GEMS. Nonetheless, GEMS allows to simulate several nanoseconds of dynamics for systems consisting of thousands of atoms with *ab initio* accuracy (it may be possible to combine GEMS with other ML methods to achieve further speed-ups, e.g. by allowing larger time steps during the dynamics [41]). Furthermore, GEMS like every other MLFF may lead to unphysical dynamics, if *not properly* trained (see e.g. Ref. 23 for a discussion of such phenomena). As a rule, MLFF simulations should therefore always be subjected to more scrutiny than re-

sults from mechanistic FFs. In particular, the resulting trajectories need to be carefully checked for unphysical bond breaking or formation, or otherwise unphysically distorted conformations, which are prevented in traditional FFs by construction. Nevertheless it should be emphasized again that compared to simulations with a conventional FF, GEMS offers highly improved accuracy as well as enables to study chemical transformations such as the making and breaking of chemical bonds and proton transfer processes.

Another advantage of using accurate MLFFs is the availability of arbitrary derivatives – including the potential to obtain alchemical derivatives [42, 43]. This may enable the *optimization* of accessible observables, such as docking/binding energies, with respect to local (nearly isosteric) mutations. In a more conventional approach, MLFFs can be used to describe the effects of mutations via thermodynamic integration as regularly performed with classical FFs [44–46]. Given the incorporation of non-locality in the present methodology, such analyses could naturally account for longer-range phenomena like (static) allosteric effects and the inherent non-additivity of interactions known to be relevant for the free energy of binding or stability [47]. In a similar vein, this may allow to perform sensitivity analyses or engage explainability methods (see, e.g., Ref. 48) to identify allosteric hotspots and networks, which have also been speculated to play an important role for the evolutionary aspects of proteins and the biomolecular machinery [49, 50]. Again, we would like to stress that such studies and the above approaches are not limited to biomolecular systems. They may equally well be applied in materials design; for example, studying and optimizing point defects in solid state systems as relevant to the design of quantum materials.

Finally, we would like to highlight a promising application of GEMS to modeling protein-protein interactions. Fig. 5 shows the binding curves of the angiotensin converting enzyme 2 (ACE2) and the receptor binding domain (RBD) of the spike protein of SARS-CoV-1 and SARS-CoV-2 variants using either AmberFF or GEMS (in gas phase). Here, as expected from experimental evidence [51] we observe a stronger binding of the SARS-CoV-2 both for the classical FF as well as GEMS. Interestingly, however, GEMS yields a substantially stronger binding by  $-1.1$  eV. While the obtained binding energies do not account for solvation or entropic effects and cannot be directly compared to experimental binding affinities,

this application provides evidence of the importance of *ab initio* accuracy when studying interactions between complex biological systems. We therefore would like to stress the high promise of GEMS for enabling quantum-mechanical insight in broad application domains across enzyme and protein chemistry or heterogeneous materials. Although top-down fragments in this work are system-specific, in the future, they may be generated to cover a wider range of systems and enable GEMS simulations with a chemically transferable and size-extensive “universal” machine-learned force field.

## Materials and methods

### Construction of fragment data

**Bottom-up fragments** The construction of bottom-up fragments follows an approach similar in spirit to the one described by Huang et al. [14]. Ignoring hydrogen atoms, increasingly large chemical graphs with the same local bonding patterns as the system of interest are constructed until a maximum number of heavy atoms is reached. This is achieved by starting from graphs consisting of a single heavy atom. Larger graphs are constructed by successively adding additional heavy atoms and pruning graphs which do not appear as substructures in the original system. Once the graphs are constructed, they are converted to bottom-up fragments by saturating all valencies with hydrogen atoms and generating the corresponding three-dimensional molecular structure (e.g. using Open Babel [52]). For all structures, multiple conformers are sampled using either MD simulations at high temperatures or normal mode sampling [53]. Here, we use the bottom-up fragments for proteins generated in earlier work [54] (see Ref. 55 for details). Since all similar local structures are covered by the same graphs, the bottom-up fragments optimally exploit any structural redundancies, often resulting in a surprisingly small number of fragments. For example, just 2 307 chemical graphs (with a maximum of eight heavy atoms) are sufficient to cover all local bonding patterns appearing in proteins consisting of the twenty natural amino acids, even when considering different protonation states and the possibility of disulfide bridges [55].

**Top-down fragments** Starting from an MD snapshot of the system of interest (sampled from conventional MD simulations, see below and Section S3 for more details), all atoms outside a spherical region around a central atom are deleted. The cutoff radius for selecting the spherical region should be chosen as large as possible, but still resulting in fragment sizes for which reference calculations are feasible (in this work, we choose 8 Å). Then, any resulting dangling single bonds on heavy atoms are saturated with hydrogen atoms. Valencies situated on hydrogen atoms or corresponding to double bonds are eliminated by including the bonded atom in the original system (outside the cutoff). This process is repeated until all valencies are saturated [24]. By choosing different central atoms, several (partially overlapping) top-down fragments can be constructed from a single configuration of the original system.

### Density Functional Theory calculations

Density Functional Theory (DFT) reference calculations were performed using the Psi4 software package [56, 57] at the PBE0/def2-TZVPP+MBD [18–21] level of theory on Google Cloud Platform (GCP). This level of theory has been found to be well-suited for modelling interactions of proteins in water [13, 58, 59]. Each fragment was run on an independent Docker container within a cloud compute engine virtual machine. We mostly used *n2d-highmem-4* and *n2-highmem-4* virtual machine instances with 4 cores, 32 GB RAM and 768 GB of disk space each, with some larger fragments being manually relaunched on higher-memory machines if they crashed with out-of-memory errors. Execution was parallelized on up to 20 000 CPU cores. Calculations were shut down if they did not complete within 21 days, which was the case for a few outliers, but median execution time per fragment was  $\approx$  48 hours.

### Training the MLFF

All MLFFs in this work use the recently proposed SpookyNet architecture (see Ref. 15 for details). We use three different trained ML models in this work, one for the simulations of all poly-alanine systems, one for the simulation of crambin in aqueous solution, and one for the gas-phase ACE2/SARS CoV-1/2 RBD binding curves shown in Fig. 5 (CoV model). The poly-alanine and CoV

models use the recommended architectural hyperparameters of  $T = 6$  interaction modules and  $F = 128$  features [15]. Due to hardware limitations when performing MD simulations for thousands of atoms, the crambin model uses  $T = 3$  interaction modules and  $F = 64$  features to reduce memory requirements. All models use a short-range cutoff of  $r_{\text{rcut}} = 10 a_0$  ( $\sim 5.29 \text{ \AA}$ ). The crambin and CoV models additionally employ a long-range cutoff of  $r_{\text{lrcut}} = 20 a_0$  ( $\sim 10.58 \text{ \AA}$ ) for the computation of the analytical electrostatic and dispersion correction terms included in the SpookyNet energy prediction (to achieve sub-quadratic scaling with respect to the number of atoms). We follow the training protocol described in Ref. 15 for fitting the parameters to reference energies, forces, and dipole moments, however, the mean squared loss function was replaced by the adaptive robust loss described in Ref. 60. All models were trained on NVIDIA V100 GPUs on GCP using the same 2 713 986 bottom-up fragments, and 45 948 (for the poly-alanine model), 5 624 (for the crambin model), or 129 942 (for the CoV model) top-down fragments. During training, structures were randomly drawn in equal amounts from bottom-up and top-down fragments, i.e. top-down fragments were oversampled to mitigate the imbalance in the numbers of bottom-up/top-down fragments.

## MD simulations

**Conventional FF** All classical MD simulations have been performed with the GROMACS 2020.3 software package using NVIDIA V100 or A100 GPUs in a Kubernetes system on GCP. Throughout this work, we have employed the AMBER99SB-ILDN force field [17] for the conventional MD simulations. Standard amino acid definitions have been adapted to accommodate charged Lys +  $\text{H}^+$  termini in accordance with the AMBER99SB-ILDN parametrizations where needed. In the MD simulations of ACE2/SARS CoV-2 RBD, the binding of the  $\text{Zn}^{2+}$ -cofactor in ACE2 has been described *via* harmonic restraints to the experimentally-determined ligands in order to avoid potential shortcomings in the description of the metal–ligand interaction. All solvated systems presented in this manuscript or used for sampling representative structures for generating top-down fragments were initially resolvated, optimized to a maximum atomic force of 1000 kJ/mol/nm, and equilibrated according to the

protocol detailed in section S2. Simulations for studying non-equilibrium processes (i.e. the gas phase folding/unfolding of poly-alanine systems) have been started directly from optimized structures with velocities drawn from a Maxwell-Boltzmann distribution at twice the simulation temperature (such that the average kinetic energy during the simulation corresponds to the desired temperature [61]). The gasphase simulations have thereby been realized in a pseudo-gasphase setting as proposed and validated in Ref. 61. All constant temperature MD simulations have been performed using temperature coupling *via* stochastic velocity rescaling [62] and a Parrinello-Rahman barostat [63] has been used for NPT simulations. To speed up computations, standard MD simulations involved the commonly employed constraint of bonds involving hydrogen, while the power spectra reported in this work have been obtained from fully unconstrained simulations. The starting structures of poly-alanine systems have been generated with the Avogadro software [64] and the initial structure of crambin has been taken from PDB entry 2FD7 [31], where the incorrectly described residues (SER11 and VAL15) have been remodeled using PyMOL [65]. Our simulations of the ACE2/SARS CoV-1/2 RBD complex have been initiated from a set of representative conformations as identified in Ref. 34 or pointwise mutations thereof. Currently available experimental results on the mutations present in the  $\beta$ -,  $\gamma$ -,  $\delta$ -, and  $\epsilon$ -variants of SARS CoV-2 do not indicate considerable structural changes to the spike RBD. After partial relaxation, simple pointwise mutations of the structural representatives obtained for the  $\alpha$ -variant can thus be assumed to represent viable starting points for MD simulations of the different variants.

**GEMS** All MD simulations with the GEMS method were performed using the SchNetPack [66] MD toolbox with a timestep of 0.5 fs and without any bond constraints. Simulations for poly-alanine systems were performed on NVIDIA V100 GPUs on GCP, whereas crambin simulations were performed on NVIDIA A100 GPUs with 80GB. To mimic experimental conditions [27], the simulations of AceAla<sub>15</sub>Lys +  $\text{H}^+$  helix stability were performed in the NVE ensemble starting from an optimized structure with initial velocities drawn from a Maxwell-Boltzmann distribution at twice the simulation temperature as explained above. The folding simulations of AceAla<sub>15</sub>Nme were

performed in the NVT ensemble at 300 K starting from the optimized FES using the same method to assign initial velocities. Simulations of crambin in aqueous solution were performed in the NPT ensemble at a temperature of 300 K and a pressure of 1.01325 bar, starting from an optimized structure and initial velocities drawn from a Maxwell-Boltzmann distribution according to the simulation temperature (the first 1 ns of dynamics was discarded to allow the system to equilibrate). Constant temperature and/or pressure simulations use the Nosé-Hoover chain thermostat/barostat [67, 68] implemented in SchNetPack using a chain length of 3.

## Acknowledgments

We thank Michael Brenner for insightful comments. OTU acknowledges funding from the Swiss National Science Foundation (Grant No. P2BSP2\_188147). MG works at the BASLEARN – TU Berlin/BASF Joint Lab for Machine Learning, co-financed by TU Berlin and BASF SE. MS and AT acknowledge financial support from the Fond National de la Recherche Luxembourg (FNR) under AFR PhD grant “CNDTEC (11274975)” as well as from the European Research Council *via* ERC Consolidator Grant “BeStMo (725291)”. This work was supported in part by the German Ministry for Education and Research under Grant Nos. 01IS14013A-E, 01GQ1115, 01GQ0850, 01IS18025A, 031L0207D, and 01IS18037A. KRM was partly supported by the Institute of Information & Communications Technology Planning & Evaluation (IITP) grants funded by the Korea government (MSIT) (No. 2019-0-00079, Artificial Intelligence Graduate School Program, Korea University and No. 2022-0-00984, Development of Artificial Intelligence Technology for Personalized Plug-and-Play Explanation and Verification of Explanation). Correspondence to OTU, AT and KRM. There are no competing interests to declare. DFT reference data for training the models and scripts for running MD simulations with GEMS will be made available upon publication.

## References

[1] Martin Karplus and J Andrew McCammon. Molecular dynamics simulations of biomolecules. *Nat.*

*Struct. Biol.*, 9(9):646–652, 2002.

- [2] Erwin Schrödinger. An undulatory theory of the mechanics of atoms and molecules. *Phys. Rev.*, 28(6):1049, 1926.
- [3] François Mouvet, Justin Villard, Viacheslav Bolnykh, and Ursula Röthlisberger. Recent advances in first-principles based molecular dynamics. *Acc. Chem. Res.*, pages 3810–3823, 2022.
- [4] Roland Schulz, Benjamin Lindner, Loukas Petridis, and Jeremy C Smith. Scaling of multimillion-atom biological molecular dynamics simulation on a petascale supercomputer. *J. Chem. Theory Comput.*, 5(10):2798–2808, 2009.
- [5] David E Shaw, Martin M Deneroff, Ron O Dror, Jeffrey S Kuskin, Richard H Larson, John K Salmon, Cliff Young, Brannon Batson, Kevin J Bowers, Jack C Chao, et al. Anton, a special-purpose machine for molecular dynamics simulation. *Commun. ACM*, 51(7):91–97, 2008.
- [6] Hans Martin Senn and Walter Thiel. QM/MM methods for biomolecular systems. *Angew. Chem., Int. Ed.*, 48(7):1198–1229, 2009.
- [7] Heather J Kulik, Jianyu Zhang, Judith P Klinman, and Todd J Martínez. How large should the QM region be in QM/MM calculations? The case of catechol O-methyltransferase. *J. Phys. Chem. B*, 120(44):11381–11394, 2016.
- [8] Oliver T Unke, Stefan Chmiela, Huziel E Saucedo, Michael Gastegger, Igor Poltavsky, Kristof T Schütt, Alexandre Tkatchenko, and Klaus-Robert Müller. Machine learning force fields. *Chem. Rev.*, 121(16):10142–10186, 2021.
- [9] Uxía Rivero, Oliver T Unke, Markus Meuwly, and Stefan Willitsch. Reactive atomistic simulations of Diels-Alder reactions: The importance of molecular rotations. *J. Chem. Phys.*, 151(10):104301, 2019.
- [10] Huziel E Saucedo, Stefan Chmiela, Igor Poltavsky, Klaus-Robert Müller, and Alexandre Tkatchenko. Molecular force fields with gradient-domain machine learning: Construction and application to dynamics

- of small molecules with coupled cluster forces. *J. Chem. Phys.*, 150(11):114102, 2019.
- [11] Weile Jia, Han Wang, Mohan Chen, Denghui Lu, Lin Lin, Roberto Car, E Weinan, and Linfeng Zhang. Pushing the limit of molecular dynamics with *ab initio* accuracy to 100 million atoms with machine learning. In *SC20: International Conference for High Performance Computing, Networking, Storage and Analysis*, pages 1–14. IEEE, 2020.
- [12] Mariana Rossi, Wei Fang, and Angelos Michaelides. Stability of complex biomolecular structures: van der Waals, hydrogen bond cooperativity, and nuclear quantum effects. *J. Phys. Chem. Lett.*, 6(21):4233–4238, 2015. doi: 10.1021/acs.jpcclett.5b01899.
- [13] Martin Stöhr and Alexandre Tkatchenko. Quantum mechanics of proteins in explicit water: The role of plasmon-like solute-solvent interactions. *Sci. Adv.*, 5(12):eaax0024, 2019.
- [14] Bing Huang and O Anatole von Lilienfeld. Quantum machine learning using atom-in-molecule-based fragments selected on the fly. *Nat. Chem.*, 12(10):945–951, 2020.
- [15] Oliver T Unke, Stefan Chmiela, Michael Gastegger, Kristof T Schütt, Huziel E Sauceda, and Klaus-Robert Müller. SpookyNet: Learning force fields with electronic degrees of freedom and nonlocal effects. *Nat. Commun.*, 12:7273, 2021.
- [16] Tsz Wai Ko, Jonas A Finkler, Stefan Goedecker, and Jörg Behler. A fourth-generation high-dimensional neural network potential with accurate electrostatics including non-local charge transfer. *Nat. Commun.*, 12(1):1–11, 2021.
- [17] Kresten Lindorff-Larsen, Stefano Piana, Kim Palmo, Paul Maragakis, John L. Klepeis, Ron O. Dror, and David E. Shaw. Improved side-chain torsion potentials for the Amber ff99SB protein force field. *Proteins*, 78(8):1950–1958, 2010. ISSN 08873585. doi: 10.1002/prot.22711.
- [18] Carlo Adamo and Vincenzo Barone. Toward reliable density functional methods without adjustable parameters: The PBE0 model. *J. Chem. Phys.*, 110(13):6158–6170, 1999.
- [19] Florian Weigend and Reinhart Ahlrichs. Balanced basis sets of split valence, triple zeta valence and quadruple zeta valence quality for H to Rn: Design and assessment of accuracy. *Phys. Chem. Chem. Phys.*, 7(18):3297–3305, 2005.
- [20] Alexandre Tkatchenko, Robert A DiStasio Jr, Roberto Car, and Matthias Scheffler. Accurate and efficient method for many-body van der Waals interactions. *Phys. Rev. Lett.*, 108(23):236402, 2012.
- [21] Alberto Ambrosetti, Anthony M Reilly, Robert A DiStasio Jr, and Alexandre Tkatchenko. Long-range correlation energy calculated from coupled atomic response functions. *J. Chem. Phys.*, 140:18A508, 2014.
- [22] Jörg Behler. Representing potential energy surfaces by high-dimensional neural network potentials. *J. Condens. Matter Phys.*, 26(18):183001, 2014.
- [23] Sina Stocker, Johannes Gasteiger, Florian Becker, Stephan Günemann, and Johannes Margraf. How robust are modern graph neural network potentials in long and hot molecular dynamics simulations? *ChemRxiv preprint*, 2022. doi: 10.26434/chemrxiv-2022-mc4gb.
- [24] Michael Gastegger, Jörg Behler, and Philipp Marquetand. Machine learning molecular dynamics for the simulation of infrared spectra. *Chem. Sci.*, 8(10):6924–6935, 2017.
- [25] Dmitriy Frishman and Patrick Argos. Knowledge-based protein secondary structure assignment. *Proteins*, 23(4):566–579, 1995.
- [26] Changmoon Park and William A Goddard. Stabilization of  $\alpha$ -helices by dipole-dipole interactions within  $\alpha$ -helices. *J. Phys. Chem. B*, 104(32):7784–7789, 2000.
- [27] Motoya Kohtani, Thaddeus C Jones, Jean E Schneider, and Martin F Jarrold. Extreme stability of an unsolvated  $\alpha$ -helix. *J. Am. Chem. Soc.*, 126(24):7420–7421, 2004.
- [28] Alexandre Tkatchenko, Mariana Rossi, Volker Blum, Joel Ireta, and Matthias Scheffler. Unraveling the

- stability of polypeptide helices: Critical role of van der Waals interactions. *Phys. Rev. Lett.*, 106(11): 118102, 2011.
- [29] Igor A Topol, Stanley K Burt, Eugen Deretey, Ting-Hua Tang, Andras Perczel, Alexander Rashin, and Imre G Csizmadia.  $\alpha$ - and  $3_{10}$ -helix interconversion: A quantum-chemical study on polyalanine systems in the gas phase and in aqueous solvent. *J. Am. Chem. Soc.*, 123(25):6054–6060, 2001.
- [30] Clara D. Craver. *The Coblenz society desk book of infrared spectra*. National Standard Reference Data System, 1977.
- [31] Duhee Bang, Valentina Tereshko, Anthony A Kossiakoff, and Stephen BH Kent. Role of a salt bridge in the model protein crambin explored by chemical protein synthesis: X-ray structure of a unique protein analogue, [V15A]crambin- $\alpha$ -carboxamide. *Mol. Biosyst.*, 5(7):750–756, 2009.
- [32] Leland McInnes, John Healy, and James Melville. UMAP: Uniform manifold approximation and projection for dimension reduction. *arXiv preprint arXiv:1802.03426*, 2018.
- [33] Martin Thomas, Martin Brehm, Reinhold Fligg, Peter Vöhringer, and Barbara Kirchner. Computing vibrational spectra from ab initio molecular dynamics. *Phys. Chem. Chem. Phys.*, 15(18):6608–6622, 2013.
- [34] Julián M. Delgado, Nalvi Duro, David M. Rogers, Alexandre Tkatchenko, Sagar A. Pandit, and Sameer Varma. Molecular basis for higher affinity of SARS-CoV-2 spike RBD for human ACE2 receptor. *Proteins*, 89(9):1134–1144, 2021. doi: 10.1002/prot.26086.
- [35] Ronald M. Levy, David Perahia, and Martin Karplus. Molecular dynamics of an  $\alpha$ -helical polypeptide: Temperature dependence and deviation from harmonic behavior. *Proc. Natl. Acad. Sci. U. S. A.*, 79(4):1346–1350, 1982. doi: 10.1073/pnas.79.4.1346.
- [36] J Andrew McCammon, Bruce R Gelin, and Martin Karplus. Dynamics of folded proteins. *Nature*, 267(5612):585–590, 1977.
- [37] DC Phillips. *Biomolecular Stereodynamics*. Adenine Press: Guilderland, NY, 1981.
- [38] Cyrus Levinthal. Are there pathways for protein folding? *J. Chim. Phys.*, 65:44–45, 1968.
- [39] Huziel E Saucedo, Valentin Vassilev-Galindo, Stefan Chmiela, Klaus-Robert Müller, and Alexandre Tkatchenko. Dynamical strengthening of covalent and non-covalent molecular interactions by nuclear quantum effects at finite temperature. *Nat. Commun.*, 12:442, 2021.
- [40] Berk Hess, Carsten Kutzner, David Van Der Spoel, and Erik Lindahl. GROMACS 4: Algorithms for highly efficient, load-balanced, and scalable molecular simulation. *J. Chem. Theory Comput.*, 4(3): 435–447, 2008.
- [41] Ludwig Winkler, Klaus-Robert Müller, and Huziel E Saucedo. Super-resolution in molecular dynamics trajectory reconstruction with bi-directional neural networks. *arXiv preprint arXiv:2201.01195*, 2022.
- [42] Karthikeyan Saravanan, John R Kitchin, O Anatole Von Lilienfeld, and John A Keith. Alchemical predictions for computational catalysis: Potential and limitations. *J. Phys. Chem. Lett.*, 8(20):5002–5007, 2017.
- [43] Daniel Sheppard, Graeme Henkelman, and O Anatole von Lilienfeld. Alchemical derivatives of reaction energetics. *J. Chem. Phys.*, 133(8):084104, 2010.
- [44] J. Ramón Blas, Manuel Márquez, Jonathan L. Sessler, F. Javier Luque, and Modesto Orozco. Theoretical study of anion binding to calix[4]pyrrole: The effects of solvent, fluorine substitution, cosolute, and water traces. *J. Am. Chem. Soc.*, 124(43):12796–12805, 2002. doi: 10.1021/ja020318m.
- [45] Frank R. Beierlein, G. Geoff Kneale, and Timothy Clark. Predicting the effects of basepair mutations in DNA-protein complexes by thermodynamic integration. *Biophys. J.*, 101(5):1130–1138, 2011. doi: 10.1016/j.bpj.2011.07.003.

- [46] Miroslav Krepl, Michal Otyepka, Pavel Banáš, and Jiří Šponer. Effect of guanine to inosine substitution on stability of canonical DNA and RNA duplexes: Molecular dynamics thermodynamics integration study. *J. Phys. Chem. B*, 117(6):1872–1879, 2013. doi: 10.1021/jp311180u.
- [47] Enrico Di Cera. Site-specific thermodynamics: Understanding cooperativity in molecular recognition. *Chem. Rev.*, 98(4):1563–1592, 1998. doi: 10.1021/cr960135g.
- [48] Wojciech Samek, Grégoire Montavon, Sebastian Lapuschkin, Christopher J Anders, and Klaus-Robert Müller. Explaining deep neural networks and beyond: A review of methods and applications. *Proceedings of the IEEE*, 109(3):247–278, 2021.
- [49] Steve W Lockless and Rama Ranganathan. Evolutionarily conserved pathways of energetic connectivity in protein families. *Science*, 286(5438):295–299, 1999.
- [50] Arjun S. Raman, K. Ian White, and Rama Ranganathan. Origins of allostery and evolvability in proteins: A case study. *Cell*, 166(2):468–480, 2016. doi: 10.1016/j.cell.2016.05.047.
- [51] Daniel Wrapp, Nianshuang Wang, Kizzmekia S. Corbett, Jory A. Goldsmith, Ching-Lin Hsieh, Olubukola Abiona, Barney S. Graham, and Jason S. McLellan. Cryo-EM structure of the 2019-nCoV spike in the prefusion conformation. *Science*, 367(6483):1260–1263, 2020. doi: 10.1126/science.abb2507.
- [52] Noel M O’Boyle, Michael Banck, Craig A James, Chris Morley, Tim Vandermeersch, and Geoffrey R Hutchison. Open Babel: An open chemical toolbox. *J. Cheminformatics*, 3(1):1–14, 2011.
- [53] Justin S Smith, Olexandr Isayev, and Adrian E Roitberg. ANI-1: An extensible neural network potential with DFT accuracy at force field computational cost. *Chem. Sci.*, 8(4):3192–3203, 2017.
- [54] OT Unke and M Meuwly. Solvated protein fragments data set. <https://doi.org/10.5281/zenodo.2605371>, 2019.
- [55] Oliver T Unke and Markus Meuwly. PhysNet: A neural network for predicting energies, forces, dipole moments, and partial charges. *J. Chem. Theory Comput.*, 15(6):3678–3693, 2019.
- [56] Robert M. Parrish, Lori A. Burns, Daniel G. A. Smith, Andrew C. Simmonett, A. Eugene DePrince, Edward G. Hohenstein, Uğur Bozkaya, Alexander Yu. Sokolov, Roberto Di Remigio, Ryan M. Richard, Jérôme F. Gonthier, Andrew M. James, Harley R. McAlexander, Ashutosh Kumar, Masaaki Saitow, Xiao Wang, Benjamin P. Pritchard, Prakash Verma, Henry F. Schaefer, Konrad Patkowski, Rollin A. King, Edward F. Valeev, Francesco A. Evangelista, Justin M. Turney, T. Daniel Crawford, and C. David Sherrill. Psi4 1.1: An open-source electronic structure program emphasizing automation, advanced libraries, and interoperability. *J. Chem. Theory Comput.*, 13(7):3185–3197, 2017.
- [57] Daniel G. A. Smith, Lori A. Burns, Dominic A. Sirianni, Daniel R. Nascimento, Ashutosh Kumar, Andrew M. James, Jeffrey B. Schriber, Tianyuan Zhang, Boyi Zhang, Adam S. Abbott, Eric J. Berquist, Marvin H. Lechner, Leonardo A. Cunha, Alexander G. Heide, Jonathan M. Waldrop, Tyler Y. Takeshita, Asem Alenaizan, Daniel Neuhauser, Rollin A. King, Andrew C. Simmonett, Justin M. Turney, Henry F. Schaefer, Francesco A. Evangelista, A. Eugene DePrince, T. Daniel Crawford, Konrad Patkowski, and C. David Sherrill. Psi4NumPy: An interactive quantum chemistry programming environment for reference implementations and rapid development. *J. Chem. Theory Comput.*, 14(7):3504–3511, 2018.
- [58] Robert A DiStasio Jr, Biswajit Santra, Zhaofeng Li, Xifan Wu, and Roberto Car. The individual and collective effects of exact exchange and dispersion interactions on the ab initio structure of liquid water. *J. Chem. Phys.*, 141(8):084502, 2014.
- [59] Franziska Schubert, Mariana Rossi, Carsten Baldauf, Kevin Pagel, Stephan Warnke, Gert von Helden, Frank Filsinger, Peter Kupser, Gerard Meijer, Mario Salwiczek, et al. Exploring the conformational preferences of 20-residue peptides in isolation: Ac-Ala<sub>19</sub>-Lys + H<sup>+</sup> vs. Ac-Lys-Ala<sub>19</sub> + H<sup>+</sup> and the current



- reach of DFT. *Phys. Chem. Chem. Phys.*, 17(11): 7373–7385, 2015.
- [60] Jonathan T Barron. A general and adaptive robust loss function. In *Proc. IEEE Int. Conf. Comput. Vis.*, pages 4331–4339, 2019.
- [61] Lars Konermann, Haidy Metwally, Robert G. McAllister, and Vlad Popa. How to run molecular dynamics simulations on electrospray droplets and gas phase proteins: Basic guidelines and selected applications. *Methods*, 144:104–112, 2018. ISSN 10462023. doi: 10.1016/j.ymeth.2018.04.010.
- [62] Giovanni Bussi, Davide Donadio, and Michele Parrinello. Canonical sampling through velocity rescaling. *J. Chem. Phys.*, 126(1):014101, 2007. ISSN 0021-9606. doi: 10.1063/1.2408420.
- [63] M. Parrinello and A. Rahman. Polymorphic transitions in single crystals: A new molecular dynamics method. *J. Appl. Phys.*, 52(12):7182–7190, 1981. ISSN 0021-8979. doi: 10.1063/1.328693.
- [64] Marcus D Hanwell, Donald E Curtis, David C Lonie, Tim Vandermeersch, Eva Zurek, and Geoffrey R Hutchison. Avogadro: an advanced semantic chemical editor, visualization, and analysis platform. *J. Cheminformatics*, 4(1):1–17, 2012.
- [65] Warren L DeLano et al. PyMOL: An open-source molecular graphics tool. *CCP4 Newsl. Protein Crystallogr.*, 40(1):82–92, 2002.
- [66] KT Schütt, Pan Kessel, Michael Gastegger, KA Nicoli, Alexandre Tkatchenko, and K-R Müller. SchNetPack: A deep learning toolbox for atomistic systems. *J. Chem. Theory Comput.*, 15(1):448–455, 2018.
- [67] Douglas J Tobias, Glenn J Martyna, and Michael L Klein. Molecular dynamics simulations of a protein in the canonical ensemble. *J. Phys. Chem.*, 97(49): 12959–12966, 1993.
- [68] Glenn J Martyna, Mark E Tuckerman, Douglas J Tobias, and Michael L Klein. Explicit reversible integrators for extended systems dynamics. *Mol. Phys.*, 87(5):1117–1157, 1996.

## Supplementary Information

### S1 Background

Conventional force fields (FFs) allow to study large systems, e.g. entire viruses [69–71], in atomic detail. They achieve this remarkable efficiency by modeling chemical interactions as a sum over simple empirical terms [72–74]. However, while very efficient, their accuracy is limited [75] and they typically cannot describe chemical reactions. Although there are various efforts to increase the accuracy of classical FFs, for example by including polarization effects [76, 77] and sophisticated models for anisotropic charge distributions [78–82], or by developing reactive FFs [83, 84], they are clearly much faster to evaluate but typically cannot compete with the accuracy of machine learned force fields (MLFFs) [85–91]. Machine learning (ML) methods “learn the rules” of quantum mechanics [92] and their representation from data, allowing to skip computationally expensive *ab initio* simulations. Beyond FF construction, there are several other applications of ML to quantum chemistry (QC). One of the earliest uses of ML in QC was the exploration of chemical space [93–96]. However, ML can also be used to accelerate studies that typically rely on MD simulations or other dynamical equations [97]. For example, it can be used to directly sample equilibrium distributions [98, 99] or rare events [100], or directly predict reaction rates [101]. Further, ML is used for predicting protein structure [102–104], solving the Schrödinger [105–107], predicting wave functions [108–110], modelling solvated systems [111], generating molecules and solving inverse design problems [112–118], and even for planning chemical syntheses [119].

For a more detailed overview of the use of ML in molecular and material science, refer to Refs. 120–125, for an overview of applications in molecular simulations, refer to Ref. 126, and for reviews on the exploration of chemical space, refer to Refs. 127 and 128, furthermore general reviews can be found in Refs. 92, 119, 129–134.

### S2 MD simulations — Equilibration and detailed setup

After initial preparation (resolving doubly- or ill-defined residues and atom type definitions present in the original files from the respective sources specified in the main manuscript), classical molecular dynamics (MD) simulations of solvated systems were initialized by resolvating the systems in cubic simulation boxes with a minimum protein-to-box distance of 1.6 nm. Unless explicitly specified otherwise, simulation cells were solvated in TIP3P water with physiological concentrations of NaCl with excess Na<sup>+</sup>- or Cl<sup>-</sup>-ions to neutralize the simulation box where needed. The solvated structures were subsequently optimized to a maximum atomic force of 1'000 kJ/mol/nm and equilibrated in a four-step procedure consisting of (a time step of 2 fs was used in all cases):

- 1) a short NVT-simulation of 50'000 steps (simulation time 100 ps)
- 2) NPT simulation (Berendsen barostat) of 50'000 steps (100 ps)
- 3) NPT simulation (Parrinello-Rahman barostat [135]) of 100'000 steps (200 ps) with fully constrained bonds
- 4) and 100'000 steps (200 ps) with constraints on all bonds involving hydrogen.

In all equilibration runs a constant temperature thermostat with stochastic velocity rescaling [136] set to the final simulation temperature was employed. Throughout all steps, the AMBER99SB-ILDN force field[137] was used.

For AcAla<sub>15</sub>Lys-chains involving the charged LysH<sup>+</sup> terminus, topology and AMBER definitions have been adapted accordingly using the default AMBER99SB-ILDN parametrization.

For the gasphase AcAla<sub>15</sub>Lys+H<sup>+</sup>, we adopted pseudo-gasphase settings as detailed in Ref. 138 using maximal

unit cells while disabling particle-mesh Ewald electrostatics. The constant temperature (pseudo-)gasphase simulations were prepared by structure optimization (maximum atomic force of 1'000 kJ/mol/nm). The reported simulations were then run in an NVT ensemble initialized with velocities randomly drawn from a Maxwell-Boltzmann distribution corresponding to twice the simulation temperature.

### S3 Sampling structures for top-down fragmentation

To train a model that can be used to simulate trajectories of a particular system of interest, we want to train it on a diverse set of top-down fragments representative of a variety of conformations. The general strategy is to cluster configurations that occur in classical MD simulations, select some representatives for each cluster, and then decompose the whole configurations into spherical regions that are small enough to run DFT calculations on them (top-down fragments). Different systems have different characteristics when it comes to the possible conformations:

- The poly-alanine systems unfold and thus show a lot of variation, but the overall system is comparatively small (contains few atoms).
- Crambin in aqueous solution contains many different atoms, but due to presence of three disulfide bridges, the protein itself shows only minimal variations, mainly determined by the states of the disulfide bridges, so clustering is straightforward.

#### Poly-alanine systems

In our classical MD simulation of AceAla<sub>15</sub>Nme and AceAla<sub>n</sub>Lys + H<sup>+</sup> in solution at temperatures 280K, 300K, and 310K, (2  $\mu$ s each) the poly-alanine chain did not keep a helix structure, but assumed almost arbitrary conformations. So we cannot define different well defined clusters, but we can still use a clustering algorithm to find a diverse and representative sample of the configurations seen during the trajectories.

We used affinity propagation [139] as the clustering algorithm. This algorithm takes as input a matrix specifying

“similarities” between two objects, and a “preference” that specifies the cost of adding a new cluster (which is balanced with the gain in similarity obtained by switching nearby objects to the new cluster). The output is a set of clusters with one object in each cluster designated as the representative of this cluster. The number of clusters is controlled by the relation between similarities and the preference; default choices for the preference include the median similarity and the lowest similarity, but in general the preference can be tuned to produce clusters at the desired granularity.

To compare two configurations of atoms, we move them so that the center of mass is at the origin, and then use the rotation that gives the minimal mean square distance between the atoms. The similarity is then the negative sum of the square distances.

We set the preference to -50 compared to a median similarity between -14 and -31 for the six trajectories, this gave 240 cluster for AceAla<sub>n</sub>Lys + H<sup>+</sup> molecule, and 266 cluster for the AceAla<sub>15</sub>Nme molecule.

#### Crambin

Initial structure were taken from PDB entry 2FD7. The incorrect residues SER11 and VAL15 have been remodeled using PyMOL.

Crambin has 3 disulfide bridges at atoms (NCCS:SCCN)

- 31-33-35-38:561-558-556-554
- 41-43-45-48:449-446-444-442
- 220-222-224-227:373-370-368-366

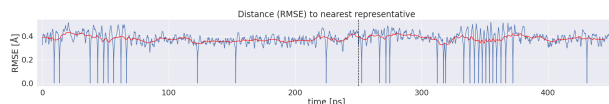
These disulfide bridges have two stable positions, in two MD simulations over 5  $\mu$ s each we observed the first and the third disulfide bridge to flip between stable positions (measured as dihedral angle of the N-C-C-S configurations). Together with a twist at an Arginine residue, these explained almost all the variations seen. We computed 22 clusters and made sure all observed variations were represented.

## S4 Comparison to ground truth for AcAla<sub>15</sub>NME trajectories

To check the accuracy of our GEMS simulation, we select samples from 100 trajectories of 2500 steps starting from a common stretched initial conformation. We subsample by only taking every second time step, which leaves 125,000 conformations. We use affinity propagation (see Section S3) to get representative samples. The similarity is the negative sum of square distances between corresponding non-hydrogen atoms, after centering the molecules and applying an optimal rotation.

However, using affinity propagation directly on these trajectories would have a large bias towards stable end conformations: Our trajectories contain stable end conformations for roughly half of the time, so affinity propagation with the default settings would spend most representatives on the stable conformations, largely ignoring the interesting folding part. To reduce this bias, we use a preprocessing step that removes conformations that have a small distance to an already selected point. (The threshold used was  $9\text{\AA}^2$  for the sum of the square distances, corresponding to  $0.3\text{\AA}$  per non-hydrogen atom for the RMSE.) This reduces the stable tails of the trajectories, but if we do this only within the trajectories, we get another bias around the common initial conformation. Computing pairwise distances for the union of all trajectories would be computationally expensive, so we use an approximation: We randomly mix all 100 trajectories and subdivide them into a partition of smaller subsets, and remove “almost duplicates” (as above) only inside each of the partitions. We then mix again and thin out again three more times. This removes most of the “almost duplicates”, and we arrive at 25,249 conformations from the original 125,000 conformations. On these 25,249 we can then run the affinity propagation; using  $\text{preference} = -1500\text{\AA}^2$  we arrive at 1554 representatives. Plotting the distance from the nearest representative (blue curve) over the trajectories now shows an even average distance: The red curve is a rolling average over 100 time points, it hovers around  $0.4\text{\AA}$ . The  $x$ -axis gives the time steps in the simulation. After every 2500 steps = 250ps the next trajectory starts, so in the image below there are data from the first two trajectories. In the blue curve, conformations that are selected as cluster representatives

can be seen as time points in which the blue curve touches the  $x$ -axis (since the distance to the closest representative is then 0). We can see that there are regions that need more representatives (e.g. when folding happens), and regions which only have occasional representatives (in the more stable end phase), but the average distance stays approximately constant.



While this takes care of any obvious bias towards common or stable positions, we also add a list of 1000 conformations that are as far away as possible from all previously selected conformations. These can be thought of as untypical or unstable conformations, and we want to make sure that our model works for them as well as it does for the maybe more typical cluster representatives.

## S5 MD simulation code

The MD simulations are performed with the SchNetPack[140] toolbox providing an interface to the Atomic Simulation Environment [141] to run MD simulations with machine learning models. SchNetPack includes a fully functional MD suite, which can be used to perform efficient MD and PIMD simulations in different ensembles. The SpookyNet [142] model is used to implement

```
schnetpack.md.calculators.MDCalculator
```

interface from SchNetPack. See figure S1 for the schematic and corresponding papers for more details. Both SpookyNet and SchNetPack are written in PyTorch and thus can be used to run MD simulations directly on GPU increasing performance (and decreasing time per simulation step) by orders on magnitude compared to CPU-based models.

## References

- [69] Peter L Freddolino, Anton S Arkhipov, Steven B Larson, Alexander McPherson, and Klaus Schulten. Molecular dynamics simulations of the com-

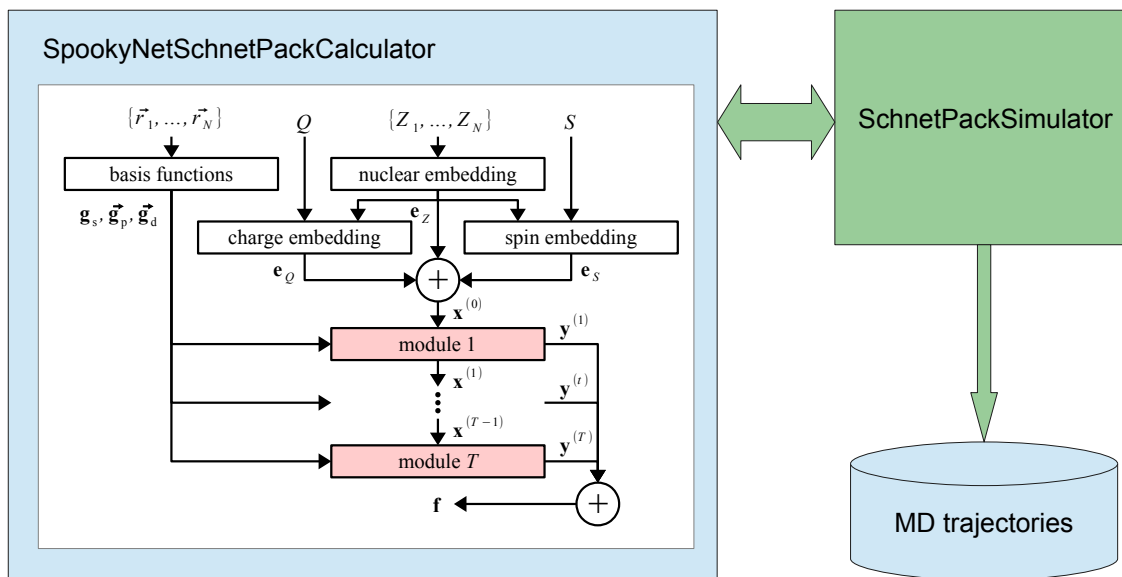


Figure S1: MD implementation: only the blue box (schNetpack.MDCalculator subclass using SpookyNet model to get forces predictions from atom positions and charges) needs to be implemented. SchNetPack Simulator takes care of running MD simulation, checkpointing and writing logs and trajectories to disk.

- plete satellite tobacco mosaic virus. *Structure*, 14(3): 437–449, 2006.
- [70] Gongpu Zhao, Juan R Perilla, Ernest L Yufenyuy, Xin Meng, Bo Chen, Jiying Ning, Jinwoo Ahn, Angela M Gronenborn, Klaus Schulten, Christopher Aiken, et al. Mature HIV-1 capsid structure by cryo-electron microscopy and all-atom molecular dynamics. *Nature*, 497(7451):643–646, 2013.
- [71] Maxwell I Zimmerman, Justin R Porter, Michael D Ward, Sukrit Singh, Neha Vithani, Artur Meller, Upasana L Mallimadugula, Catherine E Kuhn, Jonathan H Borowsky, Rafal P Wiewiora, et al. Citizen scientists create an exascale computer to combat COVID-19. *BioRxiv*, 2020.
- [72] John Edward Lennard-Jones. On the determination of molecular fields. – II. from the equation of state of a gas. *Proc. R. Soc. Lond. A*, 106(738):463–477, 1924.
- [73] MA González. Force fields and molecular dynamics simulations. In *École thématique de la Société Française de la Neutronique*, volume 12, pages 169–200. EDP Sciences, 2011.
- [74] Oliver T Unke, Debasish Koner, Sarbani Patra, Silvan Käser, and Markus Meuwly. High-dimensional potential energy surfaces for molecular simulations: From empiricism to machine learning. *Mach. Learn.: Sci. Technol.*, 1(1):13001, 2020.
- [75] Francesca Vitalini, Antonia SJS Mey, Frank Noé, and Bettina G Keller. Dynamic properties of force fields. *J. Chem. Phys.*, 142(8):02B611-1, 2015.
- [76] Thomas A Halgren and Wolfgang Damm. Polarizable force fields. *Curr. Opin. Struct. Biol.*, 11(2):236–242, 2001.
- [77] Arieh Warshel, Mitsunori Kato, and Andrei V Pisliakov. Polarizable force fields: History, test cases, and prospects. *J. Chem. Theory Comput.*, 3(6):2034–2045, 2007.
- [78] Thomas D Rasmussen, Pengyu Ren, Jay W Ponder, and Frank Jensen. Force field modeling of conforma-

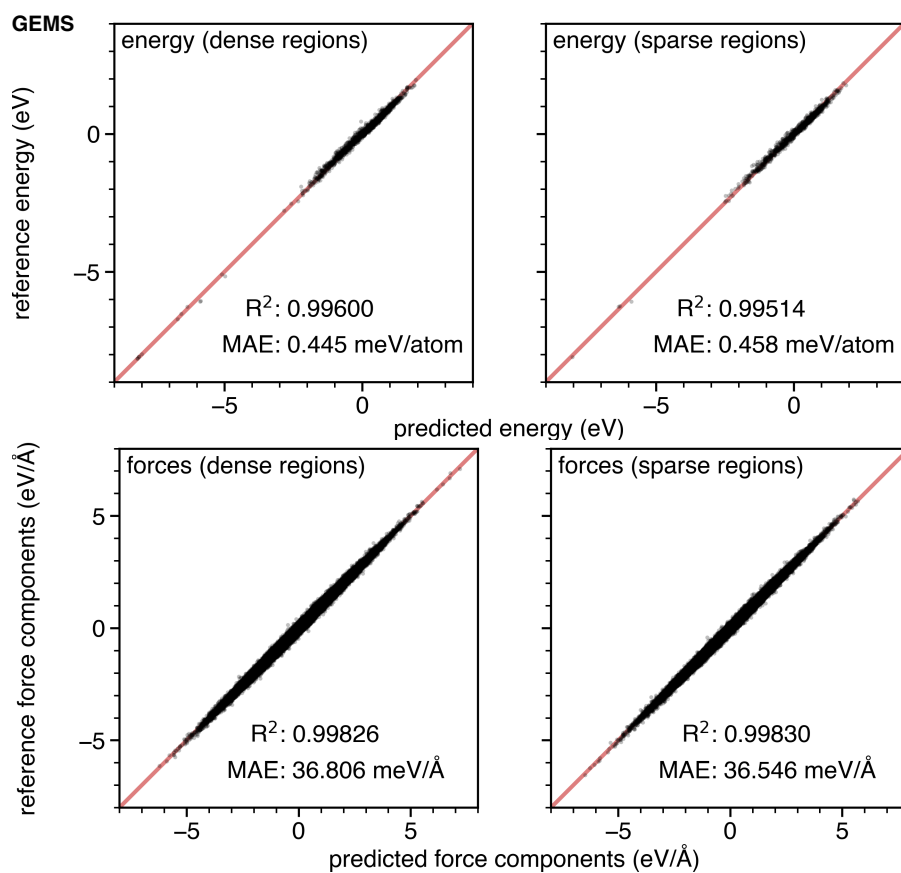


Figure S2: Correlation of predicted and *ab initio* reference (ground truth) energies and forces for AceAla<sub>15</sub>Nme conformations sampled from 100 aggregated 250 ps MD trajectories (25 ns total) in the NVT ensemble at 300 K simulated with GEMS. Conformations are sampled either from densely (1554 structures) or sparsely (1000 structures) populated regions of conformational space.

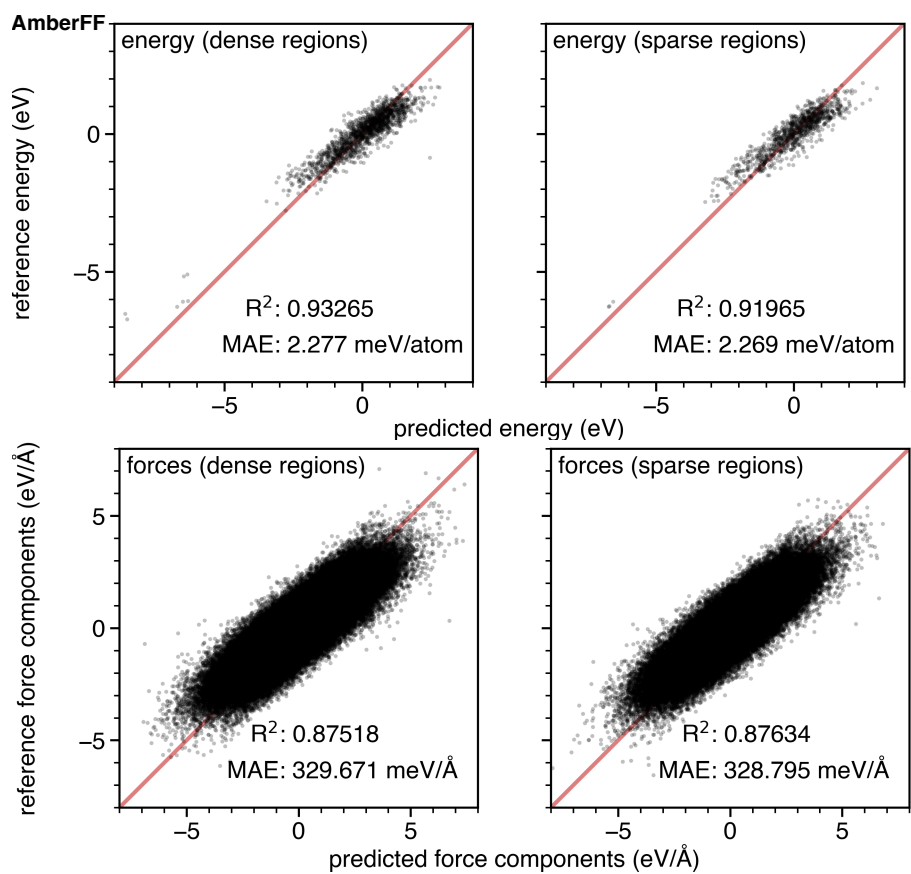


Figure S3: Same as Fig. S2, but showing the correlation for predictions with the AmberFF.

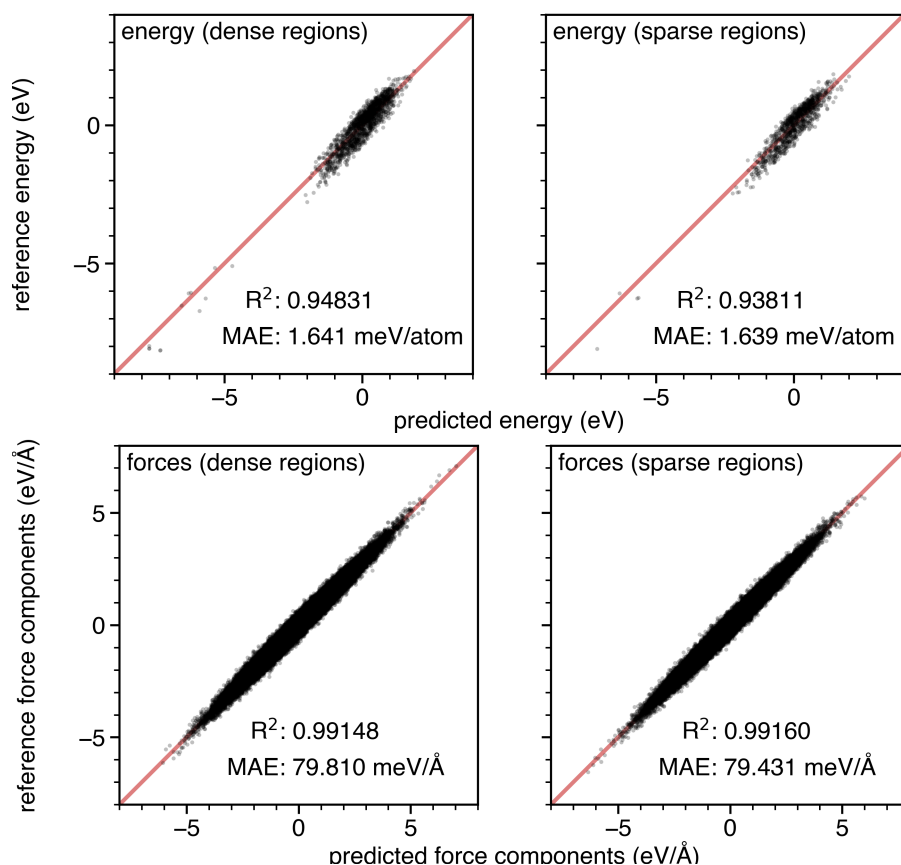


Figure S4: Same as Fig. S2, but for a GEMS model trained without top-down fragments.

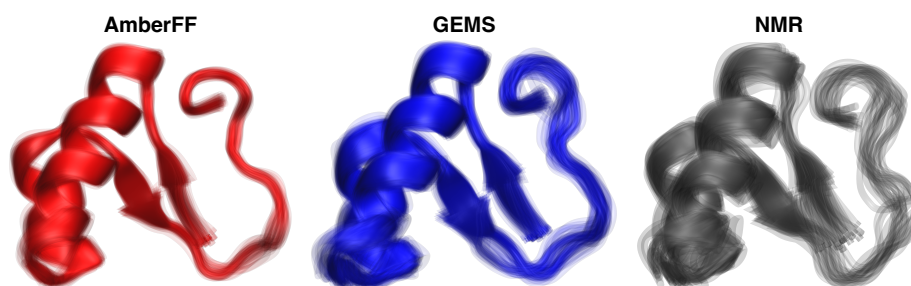


Figure S5: Overlay of representative conformations (obtained from cluster analysis) sampled during 10 ns of dynamics of crambin in aqueous solution. Simulations with GEMS (blue) lead to greater structural fluctuations compared to AmberFF (red), indicating that the protein is more flexible. For comparison, 20 low energy water refined structures of crambin in dodecylphosphocholine micelles based on NMR measurements are shown as well.[143] To allow a quantitative comparison, structures should be modelled with GEMS instead of a conventional FF when interpreting the NMR results.



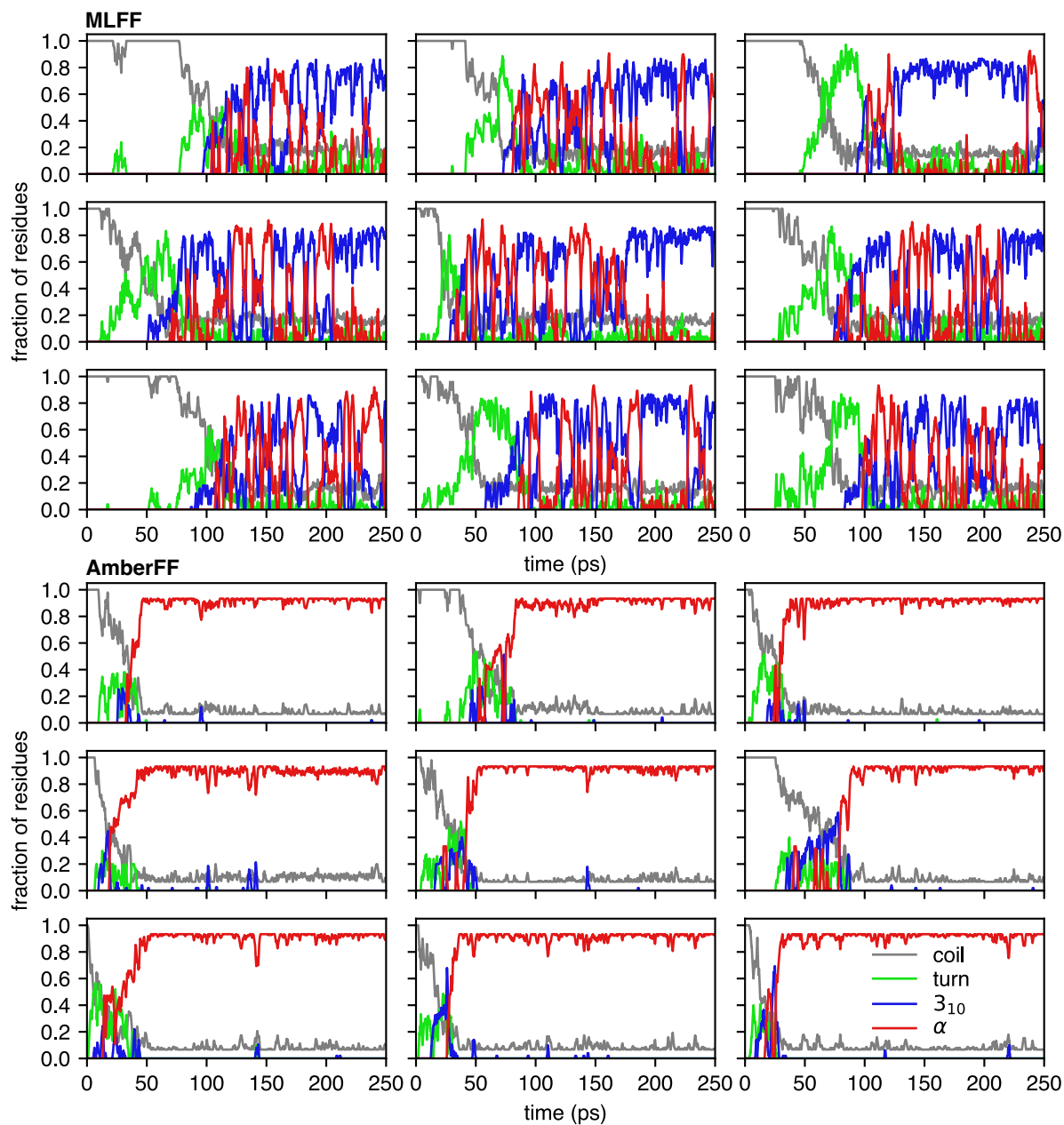


Figure S6: Secondary structural motifs (determined by STRIDE[144]) along additional folding trajectories of AcAla<sub>15</sub>NME.

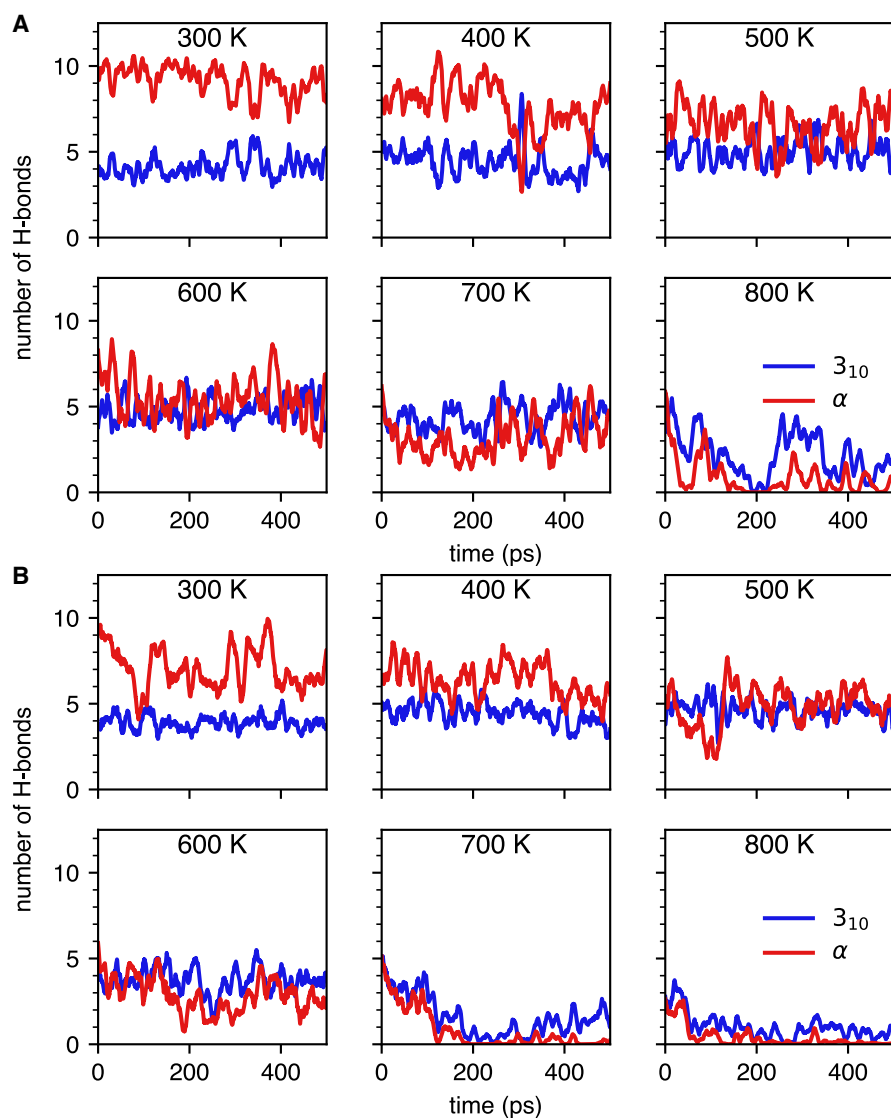


Figure S7: **(A)** Number of  $\alpha$ - and  $3_{10}$ -helical H-bonds during GEMS MD simulations of helical AceAla<sub>15</sub>Lys + H<sup>+</sup> in gas phase at different temperatures. The sharp drop in the number of H-bonds in the dynamics at 800 K indicates the formation of a random coil. **(B)** Same as panel A, but for a model trained without top-down fragments. The number of H-bonds is lower on average for all temperatures and a random coil is formed at a lower temperature.

- tional energies: Importance of multipole moments and intramolecular polarization. *Int. J. Quantum Chem.*, 107(6):1390–1395, 2007.
- [79] Michael G Darley, Chris M Handley, and Paul LA Popelier. Beyond point charges: Dynamic polarization from neural net predicted multipole moments. *J. Chem. Theory Comput.*, 4(9):1435–1448, 2008.
- [80] Shaun M Kandathil, Timothy L Fletcher, Yongna Yuan, Joshua Knowles, and Paul LA Popelier. Accuracy and tractability of a Kriging model of intramolecular polarizable multipolar electrostatics and its application to histidine. *J. Comput. Chem.*, 34(21):1850–1861, 2013.
- [81] Salvatore Cardamone, Timothy J Hughes, and Paul LA Popelier. Multipolar electrostatics. *Phys. Chem. Chem. Phys.*, 16(22):10367–10387, 2014.
- [82] Oliver T Unke, Mike Devereux, and Markus Meuwly. Minimal distributed charges: Multipolar quality at the cost of point charge electrostatics. *J. Chem. Phys.*, 147(16):161712, 2017.
- [83] Arieh Warshel and Robert M Weiss. An empirical valence bond approach for comparing reactions in solutions and in enzymes. *J. Am. Chem. Soc.*, 102(20):6218–6226, 1980.
- [84] Adri CT Van Duin, Siddharth Dasgupta, Francois Lorant, and William A Goddard. ReaxFF: A reactive force field for hydrocarbons. *J. Phys. Chem. A*, 105(41):9396–9409, 2001.
- [85] Jörg Behler and Michele Parrinello. Generalized neural-network representation of high-dimensional potential-energy surfaces. *Phys. Rev. Lett.*, 98(14):146401, 2007.
- [86] Paul LA Popelier. QCTFF: On the construction of a novel protein force field. *Int. J. Quantum Chem.*, 115(16):1005–1011, 2015.
- [87] Justin S Smith, Olexandr Isayev, and Adrian E Roitberg. ANI-1: An extensible neural network potential with DFT accuracy at force field computational cost. *Chem. Sci.*, 8(4):3192–3203, 2017.
- [88] Jörg Behler. First principles neural network potentials for reactive simulations of large molecular and condensed systems. *Angew. Chem. Int. Ed.*, 56(42):12828–12840, 2017.
- [89] Jörg Behler. Four generations of high-dimensional neural network potentials. *Chem. Rev.*, 121(16):10037–10072, 2021.
- [90] Stefan Chmiela, Alexandre Tkatchenko, Huziel E. Sauceda, Igor Poltavsky, Kristof T. Schütt, and Klaus-Robert Müller. Machine learning of accurate energy-conserving molecular force fields. *Sci. Adv.*, 3(5):e1603015, 2017. doi: 10.1126/sciadv.1603015.
- [91] Stefan Chmiela, Huziel E. Sauceda, Klaus-Robert Müller, and Alexandre Tkatchenko. Towards exact molecular dynamics simulations with machine-learned force fields. *Nat. Commun.*, 9(1):3887, 2018. doi: 10.1038/s41467-018-06169-2.
- [92] Kristof T Schütt, Stefan Chmiela, O Anatole von Lilienfeld, Alexandre Tkatchenko, Koji Tsuda, and Klaus-Robert Müller. *Machine Learning Meets Quantum Physics*, volume 968. Springer Lecture Notes in Physics, 2020. doi: 10.1007/978-3-030-40245-7.
- [93] Matthias Rupp, Alexandre Tkatchenko, Klaus-Robert Müller, and O Anatole Von Lilienfeld. Fast and accurate modeling of molecular atomization energies with machine learning. *Phys. Rev. Lett.*, 108(5):058301, 2012.
- [94] Grégoire Montavon, Matthias Rupp, Vivekanand Gobre, Alvaro Vazquez-Mayagoitia, Katja Hansen, Alexandre Tkatchenko, Klaus-Robert Müller, and O Anatole Von Lilienfeld. Machine learning of molecular electronic properties in chemical compound space. *New J. Phys.*, 15(9):095003, 2013.
- [95] Katja Hansen, Grégoire Montavon, Franziska Biegler, Siamac Fazli, Matthias Rupp, Matthias Scheffler, O Anatole Von Lilienfeld, Alexandre Tkatchenko, and Klaus-Robert Müller. Assessment and validation of machine learning methods for predicting molecular atomization energies. *J. Chem. Theory Comput.*, 9(8):3404–3419, 2013.

- [96] Katja Hansen, Franziska Biegler, Raghunathan Ramakrishnan, Wiktor Pronobis, O Anatole Von Lilienfeld, Klaus-Robert Müller, and Alexandre Tkatchenko. Machine learning predictions of molecular properties: Accurate many-body potentials and nonlocality in chemical space. *J. Phys. Chem. Lett.*, 6(12):2326–2331, 2015.
- [97] Lorenzo Boninsegna, Feliks Nüske, and Cecilia Clementi. Sparse learning of stochastic dynamical equations. *J. Chem. Phys.*, 148(24):241723, 2018.
- [98] Frank Noé, Simon Olsson, Jonas Köhler, and Hao Wu. Boltzmann generators: Sampling equilibrium states of many-body systems with deep learning. *Science*, 365(6457):eaaw1147, 2019.
- [99] Jonas Köhler, Leon Klein, and Frank Noé. Equivariant flows: Exact likelihood generative learning for symmetric densities. *arXiv preprint arXiv:2006.02425*, 2020.
- [100] Jun Zhang, Yi Isaac Yang, and Frank Noé. Targeted adversarial learning optimized sampling. *J. Phys. Chem. Lett.*, 10(19):5791–5797, 2019.
- [101] Debasish Koner, Oliver T Unke, Kyle Boe, Raymond J Bemish, and Markus Meuwly. Exhaustive state-to-state cross sections for reactive molecular collisions from importance sampling simulation and a neural network representation. *J. Chem. Phys.*, 150(21):211101, 2019.
- [102] Andrew W Senior, Richard Evans, John Jumper, James Kirkpatrick, Laurent Sifre, Tim Green, Chongli Qin, Augustin Židek, Alexander WR Nelson, Alex Bridgland, Hugo Penedones, Stig Petersen, Karen Simonyan, Steve Crossan, Pushmeet Kohli, David T Jones, David Silver, Koray Kavukcuoglu, and Demis Hassabis. Improved protein structure prediction using potentials from deep learning. *Nature*, 577(7792):706–710, 2020.
- [103] John Jumper, Richard Evans, Alexander Pritzel, Tim Green, Michael Figurnov, Olaf Ronneberger, Kathryn Tunyasuvunakool, Russ Bates, Augustin Židek, Anna Potapenko, Alex Bridgland, Clemens Meyer, Simon A A Kohl, Andrew J Ballard, Andrew Cowie, Bernardino Romera-Paredes, Stanislaw Nikolov, Rishub Jain, Jonas Adler, Trevor Back, Stig Petersen, David Reiman, Ellen Clancy, Michal Zielinski, Martin Steinegger, Michalina Pacholska, Tamas Berghammer, Sebastian Bodenstein, David Silver, Oriol Vinyals, Andrew W Senior, Koray Kavukcuoglu, Pushmeet Kohli, and Demis Hassabis. Highly accurate protein structure prediction with AlphaFold. *Nature*, 596(7873):583–589, 2021.
- [104] Kathryn Tunyasuvunakool, Jonas Adler, Zachary Wu, Tim Green, Michal Zielinski, Augustin Židek, Alex Bridgland, Andrew Cowie, Clemens Meyer, Agata Laydon, Sameer Velankar, Gerard J Kleywegt, Alex Bateman, Richard Evans, Alexander Pritzel, Michael Figurnov, Olaf Ronneberger, Russ Bates, Simon A A Kohl, Anna Potapenko, Andrew J Ballard, Bernardino Romera-Paredes, Stanislaw Nikolov, Rishub Jain, Ellen Clancy, David Reimann, Stig Petersen, Andrew W Senior, Koary Kavukcuoglu, Ewan Birney, Pushmeet Kohli, John Jumper, and Demis Hassabis. Highly accurate protein structure prediction for the human proteome. *Nature*, 596(7873):590–596, 2021.
- [105] Giuseppe Carleo and Matthias Troyer. Solving the quantum many-body problem with artificial neural networks. *Science*, 355(6325):602–606, 2017.
- [106] David Pfau, James S Spencer, Alexander GDG Matthews, and W Matthew C Foulkes. *Ab initio* solution of the many-electron Schrödinger equation with deep neural networks. *Phys. Rev. Res.*, 2(3):033429, 2020.
- [107] Jan Hermann, Zeno Schätzle, and Frank Noé. Deep-neural-network solution of the electronic Schrödinger equation. *Nat. Chem.*, 12(10):891–897, 2020.
- [108] KT Schütt, Michael Gastegger, Alexandre Tkatchenko, K-R Müller, and Reinhard J Maurer. Unifying machine learning and quantum chemistry with a deep neural network for molecular wavefunctions. *Nat. Comm.*, 10(1):1–10, 2019.
- [109] M Gastegger, A McSloy, M Luya, KT Schütt, and RJ Maurer. A deep neural network for molecular wave functions in quasi-atomic minimal basis representation. *J. Chem. Phys.*, 153(4):044123, 2020. doi:10.1063/5.0012911.

- [110] Oliver Unke, Mihail Bogojeski, Michael Gastegger, Mario Geiger, Tess Smidt, and Klaus-Robert Müller. SE(3)-equivariant prediction of molecular wavefunctions and electronic densities. *Advances in Neural Information Processing Systems*, 34, 2021.
- [111] Michael Gastegger, Kristof T Schütt, and Klaus-Robert Müller. Machine learning of solvent effects on molecular spectra and reactions. *Chem. Sci.*, 12(34):11473–11483, 2021.
- [112] Mariya Popova, Olexandr Isayev, and Alexander Tropsha. Deep reinforcement learning for *de novo* drug design. *Sci. Adv.*, 4(7):eaap7885, 2018.
- [113] Mariya Popova, Mykhailo Shvets, Junier Oliva, and Olexandr Isayev. Molecularrrnn: Generating realistic molecular graphs with optimized properties. *arXiv preprint arXiv:1905.13372*, 2019.
- [114] Niklas WA Gebauer, Michael Gastegger, and Kristof T Schütt. Generating equilibrium molecules with deep neural networks. In *NeurIPS 2018 Workshop on Machine Learning for Molecules and Materials*, 2018.
- [115] Niklas Gebauer, Michael Gastegger, and Kristof Schütt. Symmetry-adapted generation of 3d point sets for the targeted discovery of molecules. In *Adv. Neural. Inf. Process. Syst.*, pages 7566–7578, 2019.
- [116] Moritz Hoffmann and Frank Noé. Generating valid Euclidean distance matrices. *arXiv preprint arXiv:1910.03131*, 2019.
- [117] Robin Winter, Floriane Montanari, Andreas Steffen, Hans Briem, Frank Noé, and Djork-Arné Clevert. Efficient multi-objective molecular optimization in a continuous latent space. *Chem. Sci.*, 10(34):8016–8024, 2019.
- [118] Niklas WA Gebauer, Michael Gastegger, Stefaan SP Hessmann, Klaus-Robert Müller, and Kristof T Schütt. Inverse design of 3d molecular structures with conditional generative neural networks. *Nat. Commun.*, 13(1):1–11, 2022.
- [119] Felix Strieth-Kalthoff, Frederik Sandfort, Marwin HS Segler, and Frank Glorius. Machine learning the ropes: Principles, applications and directions in synthetic chemistry. *Chem. Soc. Rev.*, 49(17):6154–6168, 2020.
- [120] Anubhav Jain, Shyue Ping Ong, Geoffroy Hautier, Wei Chen, William Davidson Richards, Stephen Dacek, Shreyas Cholia, Dan Gunter, David Skinner, Gerbrand Ceder, et al. Commentary: The materials project: A materials genome approach to accelerating materials innovation. *APL Mater.*, 1(1):011002, 2013.
- [121] Christopher C Fischer, Kevin J Tibbetts, Dane Morgan, and Gerbrand Ceder. Predicting crystal structure by merging data mining with quantum mechanics. *Nat. Mater.*, 5(8):641–646, 2006.
- [122] Daniel P Tabor, Loïc M Roch, Semion K Saikin, Christoph Kreisbeck, Dennis Sheberla, Joseph H Montoya, Shyam Dwaraknath, Muratahan Aykol, Carlos Ortiz, Hermann Tribukait, et al. Accelerating the discovery of materials for clean energy in the era of smart automation. *Nat. Rev. Mater.*, 3(5):5–20, 2018.
- [123] Keith T Butler, Daniel W Davies, Hugh Cartwright, Olexandr Isayev, and Aron Walsh. Machine learning for molecular and materials science. *Nature*, 559(7715):547–555, 2018.
- [124] Phil De Luna, Jennifer Wei, Yoshua Bengio, Alán Aspuru-Guzik, and Edward Sargent. Use machine learning to find energy materials. *Nature*, 552:23–27, 2017.
- [125] Gus LW Hart, Tim Mueller, Cormac Toher, and Stefano Curtarolo. Machine learning for alloys. *Nat. Rev. Mater.*, 6(8):730–755, 2021.
- [126] Frank Noé, Alexandre Tkatchenko, Klaus-Robert Müller, and Cecilia Clementi. Machine learning for molecular simulation. *Annu. Rev. Phys. Chem.*, 71:361–390, 2020.
- [127] O Anatole von Lilienfeld, Klaus-Robert Müller, and Alexandre Tkatchenko. Exploring chemical compound space with quantum-based machine learning. *Nat. Rev. Chem.*, 4(7):347–358, 2020.

- [128] Bing Huang and O Anatole von Lilienfeld. *Ab initio* machine learning in chemical compound space. *Chem. Rev.*, 121(16):10001–10036, 2021.
- [129] O Anatole von Lilienfeld and Kieron Burke. Retrospective on a decade of machine learning for chemical discovery. *Nat. Commun.*, 11:4895, 2020.
- [130] Alexandre Tkatchenko. Machine learning for chemical discovery. *Nat. Commun.*, 11:4125, 2020.
- [131] John A Keith, Valentin Vassilev-Galindo, Bingqing Cheng, Stefan Chmiela, Michael Gastegger, Klaus-Robert Müller, and Alexandre Tkatchenko. Combining machine learning and computational chemistry for predictive insights into chemical systems. *Chem. Rev.*, 121(16):9816–9872, 2021. URL <https://pubs.acs.org/doi/abs/10.1021/acs.chemrev.1c00107>.
- [132] Aldo Glielmo, Brooke E Husic, Alex Rodriguez, Cecilia Clementi, Frank Noé, and Alessandro Laio. Unsupervised learning methods for molecular simulation data. *Chem. Rev.*, 121(16):9722–9758, 2021.
- [133] Markus Meuwly. Machine learning for chemical reactions. *Chem. Rev.*, 121(16):10218–10239, 2021.
- [134] Julia Westermayr and Philipp Marquetand. Machine learning for electronically excited states of molecules. *Chem. Rev.*, 121(16):9873–9926, 2021.
- [135] M. Parrinello and A. Rahman. Polymorphic transitions in single crystals: A new molecular dynamics method. *J. Appl. Phys.*, 52(12):7182–7190, 1981. ISSN 0021-8979. doi: 10.1063/1.328693.
- [136] Giovanni Bussi, Davide Donadio, and Michele Parrinello. Canonical sampling through velocity rescaling. *J. Chem. Phys.*, 126(1):014101, 2007. ISSN 0021-9606. doi: 10.1063/1.2408420.
- [137] Kresten Lindorff-Larsen, Stefano Piana, Kim Palmo, Paul Maragakis, John L. Klepeis, Ron O. Dror, and David E. Shaw. Improved side-chain torsion potentials for the Amber ff99SB protein force field. *Proteins*, 78(8):1950–1958, 2010. ISSN 08873585. doi: 10.1002/prot.22711.
- [138] Lars Konermann, Haidy Metwally, Robert G. McAllister, and Vlad Popa. How to run molecular dynamics simulations on electrospray droplets and gas phase proteins: Basic guidelines and selected applications. *Methods*, 144:104–112, 2018. ISSN 10462023. doi: 10.1016/j.ymeth.2018.04.010.
- [139] Brendan J Frey and Delbert Dueck. Clustering by passing messages between data points. *Science*, 315(5814):972–976, 2007.
- [140] KT Schütt, Pan Kessel, Michael Gastegger, KA Nicoli, Alexandre Tkatchenko, and K-R Müller. SchNetPack: A deep learning toolbox for atomistic systems. *J. Chem. Theory Comput.*, 15(1):448–455, 2018.
- [141] Ask Hjorth Larsen, Jens Jørgen Mortensen, Jakob Blomqvist, Ivano E Castelli, Rune Christensen, Marcin Dułak, Jesper Friis, Michael N Groves, Bjørk Hammer, Cory Hargus, et al. The atomic simulation environment – a Python library for working with atoms. *J. Phys. Condens. Matter*, 29(27):273002, 2017.
- [142] Oliver T Unke, Stefan Chmiela, Michael Gastegger, Kristof T Schütt, Huziel E Sauceda, and Klaus-Robert Müller. SpookyNet: Learning force fields with electronic degrees of freedom and nonlocal effects. *Nat. Commun.*, 12:7273, 2021.
- [143] Hee-Chul Ahn, Nenad Juranić, Slobodan Macura, and John L Markley. Three-dimensional structure of the water-insoluble protein crambin in dodecylphosphocholine micelles and its minimal solvent-exposed surface. *J. Am. Chem. Soc.*, 128(13):4398–4404, 2006.
- [144] Dmitriy Frishman and Patrick Argos. Knowledge-based protein secondary structure assignment. *Proteins*, 23(4):566–579, 1995.